October 23, 1974

To the Graduate Council:

I am submitting herewith a thesis written by João Paulo Trincheiras Tôrres entitled "An Experimental Investigation of the Acoustic Properties of Multitube Model Air Jets with and without Swirl." I recommend that it be accepted in partial fulfillment of the requirements for the degree of Master of Science, with a major in Aerospace Engineering.

James R. Maus, Jr.
James R. Maus, Jr., Major Professor

We have read this thesis
and recommend its acceptance:

Conley Powell

Grant J. Patterson

Accepted for the Council:

Hilton A. Smith
Vice Chancellor
Graduate Studies and Research

# AN EXPERIMENTAL INVESTIGATION OF THE ACOUSTIC PROPERTIES OF MULTITUBE MODEL AIR JETS WITH AND WITHOUT SWIRL

A Thesis

Presented for the

Master of Science

Degree

The University of Tennessee

João Paulo Trincheiras Tôrres

December 1974

## ACKNOWLEDGMENTS

The author of this study wishes to express his gratitude to his advisor and committee chairman, Dr. James R. Maus, Jr., for his advice in this investigation. This work was supported by a grant from the Federal Aviation Administration (FAA) at The University of Tennessee Space Institute, under Contract DOT-FA72WA-3053.

Special thanks go to Drs. T. Conley Powell and Grant T. Patterson, members of the author's committee, for their valuable comments on this thesis.

The author is also indebted to Mr. J. R. Goodman, laboratory technician, and fellow students M. C. Joshi and I. U. Borchers for many helpful suggestions and help in data collection.

The author wishes to thank Mrs. Judy Wright for her typing efforts.

The author's family deserves much of the credit for their love and confidence.



1176583

## ABSTRACT

The purpose of this study is to assess the aero-acoustic characteristics of multitube nozzles with and without swirling flow. Comparison of these configurations with a convergent (3 cm diameter) circular nozzle of identical exhaust area was made throughout.

Experiments conducted in the reverberation room and the free field showed that not only the multitube nozzles with and without swirl are, in general, quieter (at high subsonic Mach numbers) than the single circular nozzle of identical exhaust area, but they also introduce a frequency shift of the sound to higher frequencies and affect the directivity of the radiated sound power.

An estimate of the thrust loss for swirling flows was also conducted giving about a 15.8 percent reduction of thrust for the highest degree of swirl vanes (i.e., 45 degrees).

TABLE OF CONTENTS


| CHAPTER | | PAGE |
|---|---|---|
| I. | INTRODUCTION | 1 |
| | The Aircraft Noise Problem | 1 |
| | Previous Work | 1 |
| | Present Research | 3 |
| II. | THEORY AND ANALYSIS OF MULTITUBE NOZZLES | 4 |
| | Acoustic Properties | 4 |
| | General | 4 |
| | Free-field | 8 |
| | Fluid Dynamic Relations | 9 |
| III. | EQUIPMENT, METHODS AND EXPERIMENTAL FACILITIES | 14 |
| | The Nozzles | 14 |
| | Reverberation Room and Reverberation Times | 19 |
| | The Free-Field | 32 |
| | Air Supply and Flow Controls | 35 |
| | Acoustic Instrumentation | 36 |
| | The Shadowgraph Method | 40 |
| IV. | DATA AND RESULTS | 43 |
| | Introduction | 43 |
| | Reverberation Room Data | 44 |
| | Free-Field Data | 62 |
| V. | DISCUSSION, CONCLUSIONS AND RECOMMENDATIONS | 73 |
| | Discussion of Results | 73 |
| | Reverberation room | 73 |

CHAPTER PAGE

Free-field . . . . . 76

Summary . . . . . 77

Suggestions for Future Work . . . . . 78

BIBLIOGRAPHY . . . . . 80

APPENDICES . . . . . 83

VITA . . . . . 98

## LIST OF TABLES


| TABLE | | PAGE |
|---|---|---|
| I. | Characteristic Frequencies of the Reverberation Room up to 250 Hertz | 24 |
| II. | One-Third Octave Bandwidth Center Frequencies | 41 |
| III. | Typical Reverberation Room Data (Test Run 162) | 89 |
| IV. | Typical Free-Field Data (Test Run 168) | 90 |
| V. | Partial Output of a Data Reduction Computer Program (Sample Data at $M_e$ = 0.9 Only) | 92 |

LIST OF FIGURES


| FIGURE | | PAGE |
|---|---|---|
| 1. | Mixing Interference with Multitube Nozzles | 6 |
| 2. | Three Centimeter Circular Nozzle | 15 |
| 3. | Multitube Nozzles I and II, with Equivalent Exhaust Area as a Three Centimeter Circular Nozzle | 16 |
| 4. | Zero Degree Turning (Guide) Vanes, also Showing the (+) Plus and (-) Minus Deflections of the Vanes | 17 |
| 5. | Multitube Adaptor Plate | 20 |
| 6. | Three Centimeter Circular Nozzle Adaptor | 21 |
| 7. | Reverberation Room (Schematically) | 22 |
| 8. | Basic Sound Recording Equipment Set-Up | 27 |
| 9. | Reverberation Times Measurement Set-Up | 28 |
| 10. | Reverberation Times Curve | 29 |
| 11. | Reverberation Room Stilling Chamber | 30 |
| 12. | Free-Field Stilling Chamber | 31 |
| 13. | Plan View of Free-Field Facility | 33 |
| 14. | Principal Planes of Symmetry of Multitube Nozzles | 34 |
| 15. | Control Board | 37 |
| 16. | Air Supply System | 38 |
| 17. | Shadowgraph Equipment (Schematically) | 39 |
| 18. | Overall Sound Power Versus Nozzle Configuration at $M_e = 0.50$ | 45 |

FIGURE PAGE

19. Overall Sound Power Versus Nozzle Configuration at $M_e$ = 0.70 . . . . . 46

20. Overall Sound Power Versus Nozzle Configuration at $M_e$ = 0.90 . . . . . 47

21. Frequency Spectra at Three Different Mach Numbers for the MT1 and the Three Centimeter Circular Nozzle . . . . . 48

22. Frequency Spectra of the MT1 and the Zero Degree Guide Vane Nozzles . . . . . 50

23. Sound Power Versus Frequency for Three Nozzle Configurations . . . . . 51

24. Noise Spectra Mean Frequency Versus Mach Number for Swirling Flows with Same Sign Spins and MT1 and Three Centimeter Circular Nozzles for Comparison . . . . . 52

25. Noise Spectra Mean Frequency Versus Mach Number for Swirling Flows with Different Sign Spins and MT1 and Three Centimeter Circular Nozzles for Comparison . . . . . 53

26. Noise Spectra Peak Frequency Versus Mach Number for Swirling Flows with Same Sign Spins and MT1 and Three Centimeter Circular Nozzles for Comparison . . . . . 55

FIGURE PAGE

27. Noise Spectra Peak Frequency Versus Mach Number for Swirling Flows with Different Sign Spins and the Three Centimeter Circular Nozzles for Comparison . . . . . 56

28. Thrust Decrease with Swirling Flow . . . . . 57

29. Mass Flow Rate Versus Pressure Ratio for Several Nozzle Configurations . . . . . 59

30. Effect of Swirl in the Flow Field . . . . . 61

31. Sound Pressure Directivity in the XY Plane of the Multitube Nozzles . . . . . 64

32. Sound Pressure Directivity in the XZ Plane of the Multitube Nozzles . . . . . 65

33. Frequency Spectra at +30 Degrees in the XZ Plane . 67

34. Frequency Spectra at +60 Degrees in the XZ Plane . 68

35. Frequency Spectra at +90 Degrees in the XZ Plane . 69

36. Frequency Spectra at -30 Degrees in the XY Plane . 70

37. Frequency Spectra at -60 Degrees in the XY Plane . 71

38. Frequency Spectra at -90 Degrees in the XY Plane . 72

39. Strouhal Number Versus Distance Downstream . . . . 94

## NOMENCLATURE

| | |
|---|---|
| $a_o$ | Ambient speed of sound |
| $a_{1,2,3}$ | Constants defined in Chapter II |
| Ar | Area |
| A | Constant defined in Chapter II |
| B | Dual nozzle spacing (inches) |
| c | Speed of sound (ft/sec) |
| $C_p$ | Specific heat at constant pressure |
| d | Nozzle diameter |
| $d_f$ | Dimensionless nozzle spacing |
| dB | Decibels |
| f | Frequency (Hertz or Hz) |
| I.D. | Inside diameter |
| log | Logarithms of base 10 |
| LP | Lighthill parameter |
| l | Characteristic length |
| M | Mach number |
| MT | Multitube nozzle |
| n | Integers |
| N | Newtons |
| OASPL | Overall sound pressure level |
| p | Pressure (PSF) |
| P | Pressure ($N/m^2$) |
| PWL | Sound power level |
| r | Radius of nozzle |

| | |
|---|---|
| RMS | Root mean square |
| R | Gas constant |
| $R_e$ | Reynolds number |
| $S_t$ | Strouhal number |
| SPL | Sound pressure level |
| t | Time (seconds) |
| T | Temperature (°R) |
| U | Velocity (ft/sec) |
| V | Velocity |
| X,Y,Z | Orthogonal coordinates |

Symbols

| | |
|---|---|
| $\omega$ | Angular velocity (radians/sec) |
| $\pi$ | 3.14159 |
| $\rho$ | Density ($lbm/ft^3$) |
| $\theta$ | Rotation in radians |
| $\nu$ | Kinematic viscosity ($ft^2/sec$) |
| $\delta$ | Boundary layer thickness (ft) |

Subscripts

| | |
|---|---|
| e | Condition at the jet exit |
| FF | Free-field |
| o | Stagnation condition |
| ref | Reference |
| RR | Reverberation room |
| sc | Stilling chamber |
| ups | Upstream |
| x,y,z | Orthogonal coordinates |
| $\infty$ | Free stream condition |

# CHAPTER I

# INTRODUCTION

## I. THE AIRCRAFT NOISE PROBLEM

With the introduction of jet engines to commercial flights, the aircraft noise has become a serious problem. In recent years, with the introduction of large airplanes and ever-escalating number of flights, the noise produced in the vicinity of airports has grown tremendously. This has prompted jet engine manufacturers to attempt to alleviate the noise problem. Their work follows usually two directions: (1) to quiet existing engines (by introducing different operating techniques and/or by modifying the flow field at the exhausts) and (2) completely designing new, quiet, engines since some of the techniques and methods used in (1) usually involve severe penalties in weight, thrust, fuel consumption and so on.

The present research concerns the first type (1) of approach to the jet noise problem.

## II. PREVIOUS WORK

The idea of multiple interfering air jets is not a new one. It has been investigated by researchers like Coles

and Callaghan (1)[1] and others. It was found that mixing interference of several jets decreases the total sound power of the configuration, when compared to a more conventional single circular nozzle with identical jet exhaust area. But it was found too that, for maximum noise reduction, several interfering jets had to be used. This, in turn, increased the complexity of the mixing nozzles. Their internal ducting losses and external in-flight drag were considerable, plus they added extra weight to the engine package.

Recently several studies have been conducted (2, 3) on single circular nozzles with rotated flows. This rotation is introduced by positioning deflected vanes upstream of the jet exit. Thrust loss can be minimized by using airfoil shaped vanes. Overall sound power reductions in the range of 2-5 dB (PWL) have been reported.

This technique looks very promising mainly due to its simplicity. Several things have already been suggested to further improve the performance of nozzles operating with swirling flows, at the expense of additional complexity of the system. It was suggested, for example, that if a feathering device could be used to bring the swirl vanes from their angle of attack ($\Delta\theta$) to 0 degrees, then an improved internal performance (lesser drag) could be achieved at cruising altitude.

---

[1]Numbers in parentheses refer to similarly numbered references in the bibliography.

## III. PRESENT RESEARCH

In the continuing search for better jet noise suppressors a combination of a twin multitube mixing nozzle with swirl was investigated.

A twin multitube (two nozzle exits) has an advantage of presenting lesser internal drag to the air flow than other configurations with several jet nozzle exits. By swirling the jets further mixing should be expected since the centrifugal forces, present in a swirling flow, will make both jets spread at a higher angle.

In addition to what was mentioned, jet to jet shielding could account for a lesser overall sound power.

Therefore by combining these effects an overall sound power reduction is expected together with a frequency shift of the sound to higher frequencies. Also, the directivity of the sound produced by the swirling jets should be affected by the combined effects already mentioned.

# CHAPTER II

## THEORY AND ANALYSIS OF MULTITUBE NOZZLES

### I. ACOUSTIC PROPERTIES

#### General

In jet noise research there are three basic methods for jet noise suppression:

1. Eliminating the sound at the source.

2. Shifting the frequency spectra of the noise to the inaudible, above 20 kHz, range.

3. Redirecting the sound where it will not be inconvenient (upwards, from a ground observer).

The last method (3) is more of a "technique" for avoiding annoyance than actual noise suppression. This investigation will deal mainly with processes (1) and (2) but some reference to (3) will also be made.

The principal source of jet engine noise is due to the turbulent mixing of the jet with the surrounding ambient air. A change in the mechanism of turbulent mixing must result in a change of noise. The sound power generated this way is proportional to (as found by Lighthill (10)):

$$\text{PWL (watts)} \sim \frac{\rho_o U_e^8 A r}{a_o^5} = LP$$

From this equation it is obvious that a reduction in jet

exhaust velocity will greatly reduce noise (since it enters to the eighth power).

A twin multitube nozzle has an increased mixing perimeter and reduced jet core length when compared to a single circular nozzle of equivalent exhaust area. Due to the proximity of the jet exits in the multitube nozzle, their air jets will intersect (Figure 1) forming a region of mixing interference between the jets which promotes a better air entrainment, causing a faster decay of velocity with distance downstream.

It is known that the high frequency noise content, in a turbulent jet flow, is generated primarily in the flow near to the nozzle exit. The further downstream, the lower will be the frequency of the jet noise generated (14).

Since the multitube jets are practically unchanged until the point that they intermix, it is reasonable to assume that the high frequency noise generated up to the point where the jets impinge will remain the same. From this it is possible to estimate the frequency below which there will be a reduction of sound power (1, 2). This calculation is carried out in Appendix E and shows that the sound frequencies below 6000 Hz will be altered by the interaction.

This reduction in the low frequency jet noise is primarily due to an effective break up of large scale eddies into smaller ones raising somewhat the high frequency content of the noise spectra.

It has been found (5) that a maximum of noise

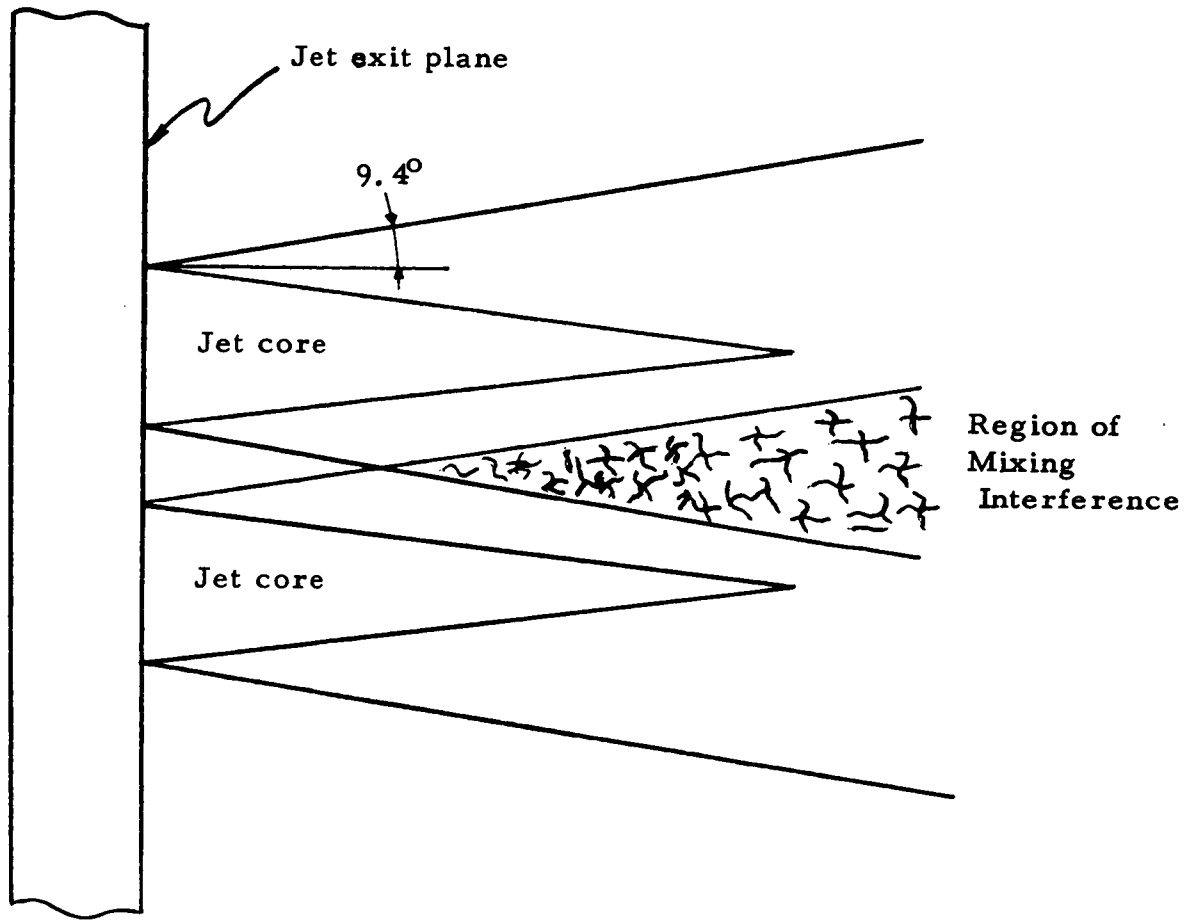


Figure 1. Mixing interference with multitube nozzles.

reduction (of the order of 2 dB) will be achieved for a twin multitube with a dimensionless nozzle spacing ($d_f$) of the order of 1.5 to 2.0. This dimensionless spacing ($d_f$) is equal to the jet centerline distance (B) divided by the nozzle diameter (d):

$$d_f = \frac{B}{d}$$

Introducing a circumferential component of velocity to exhaust from a circular nozzle also affects the noise generation. Swirling the flow of single circular jets decreases total sound power (2) due to steadier pressure fluctuations and pulsations in the rotated flow. With rotated flow, the centrifugal forces play an important role since they shift the velocity peaks outward from the jet. Also, a greater spreading angle occurs with the swirling jet than with the non-rotating jet causing a strong ambient air entrainment and an even higher decay of the jet velocity with distance downstream.

With both jets rotating (swirling), either both clockwise or one clockwise and the other counterclockwise, the mixing region will be very important since the jets have a larger spreading angle, therefore a stronger mixing interference of the two jets will occur. However, it is very difficult to mathematically formulate this problem (this was not attempted in this investigation) since the factors involved are quite complex. It involves two air jets which

intermix while having a certain degree of rotation (swirl).

The technique used to introduce swirl to the flow may be important in the generation of noise. In this study, flat splitter plates bent at certain angles were used to spin the jet. This noise, if present in the swirling flow, should be due to the vortex shedding on those plates.

Another very important point is that the energy for swirling the flow has to come from the momentum of the jet itself, in detriment of the thrust. This will be discussed in the next section.

Free-Field

Measurement of the directivity of the sound produced by the rotating (swirling) flow is essential to better understand the acoustics of these configurations. The higher mixing of both jets (due to swirl) associated with a wider spreading of each jet should contribute to an on-axis decrease of overall sound radiated, but should also increase the sideline noise.

It is believed the the 3 cm circular nozzle and an equivalent exhaust area multitube, with a small nozzle spacing (i.e., $1.25 < d_f < 2.0$), should have similar directivity patterns because in both cases circular nozzles (with either one or two jet exits) are involved and the centerline distances are small. In the limiting case, $d_f \rightarrow 1.0$ and the multitube becomes a single circular nozzle.

# II. FLUID DYNAMIC RELATIONS

An attempt to estimate the thrust loss by swirling the flow was conducted using the following approach:

An equation was derived which gives a first estimate of the thrust loss by rotating the flow assuming that the isentropic flow relations still hold for the rotated flows. No attempt was made to estimate the drag that the vanes have on the flow.

The flow undergoes a rotation $\Delta\theta$ (radians) through a length $\Delta z$ (thickness of nozzle). It is also assumed, for the simplicity in the development of the equations, that this is done in a constant area duct with a linear axial velocity profile:

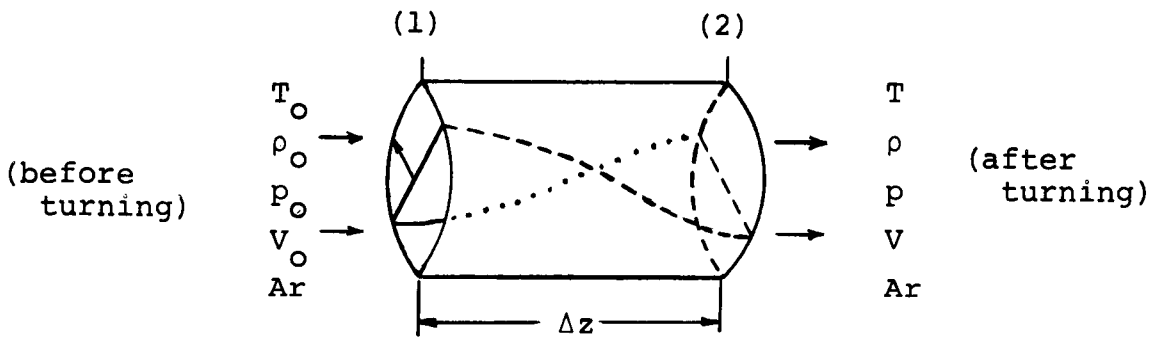


Since the area (Ar) is assumed to be constant we have:

(Continuity) $\rho V = \rho_o V_o$ (1)

(Momentum) $p + \rho V^2 = p_o + \rho_o V_o^2$ (2)

(Energy) $$C_pT + \frac{1}{2}V^2 + \frac{1}{4}r^2\omega^2 = C_pT_o + \frac{1}{2}V_o^2 \quad (3)$$

(State) $$\rho = p/RT \quad (4)$$

$$\Delta\theta = \left(\frac{\Delta z}{\frac{1}{2}(V + V_o)}\right)\frac{\omega}{2} \quad (5)$$

Equation 5 was derived using the following criteria:

The flow from stage (1) to stage (2) will have an average velocity ($V_{avg}$) given by

$$V_{avg} = \frac{V + V_o}{2}$$

The time that this flow will take to go a distance $\Delta z$ at this velocity $V_{avg}$ is then equal to

$$t = \frac{\Delta z}{t_{avg}} = \frac{\Delta z}{\frac{V + V_o}{2}}$$

During this time (t) the flow will turn (rotate) by an angle $\Delta\theta$ (in radians) such that its average angular velocity ($\bar{\omega}$) will be given simply by

$$\bar{\omega} = \frac{\Delta\theta}{t} = \frac{\Delta\theta(V + V_o)/2}{\Delta z} = \frac{\omega}{2}$$

This can be rearranged to yield Equation 5

$$\Delta\theta = \left(\frac{\Delta z}{\frac{1}{2}(V + V_o)}\right)\frac{\omega}{2}$$

Using Equations 1 through 5 an equation for V will now be derived. Substituting Equation 4 into Equations 1 and 2:

$$\frac{pV}{RT} = \rho_o V_o \tag{6}$$

$$p + \frac{pV^2}{RT} = p_o + \rho_o V_o^2 \tag{7}$$

$$\Delta\theta = \frac{\Delta z}{V + V_o}\,\omega \tag{8}$$

Solving Equation 8 for $\omega$ yields

$$\omega = \frac{\Delta\theta\,(V + V_o)}{\Delta z} \tag{9}$$

Now substituting Equation 9 into Equation 3 and solving Equation 6 for p gives

$$p = \frac{RT\rho_o V_o}{V} \tag{10}$$

$$C_p T + \frac{1}{2} V^2 + \frac{1}{4} r^2 \left[\frac{\Delta\theta\,(V + V_o)}{\Delta z}\right]^2 = C_p T_o + \frac{1}{2} V_o^2 \tag{11}$$

Replacing p (Equation 10) into Equation 7:

$$\frac{RT\rho_o V_o}{V} + \frac{RT\rho_o V_o}{V} \cdot \frac{V^2}{RT} = p_o + \rho_o V_o^2 \tag{12}$$

Rearranging Equation 12, then solving it for T, yields:

$$T = \frac{V}{R\rho_o V_o}(-VV_o\rho_o + p_o + \rho_o V_o^2) \tag{13}$$

Substituting into Equation 11:

$$\frac{C_p V}{R\rho_o V_o}(p_o + \rho_o V_o^2 - VV_o\rho_o) + \frac{1}{2}V^2 + \frac{1}{4}r^2\left[\frac{\Delta\theta(V + V_o)}{\Delta z}\right]^2$$

$$= C_p T_o + \frac{1}{2}V_o^2 \tag{14}$$

Since

$$\frac{1}{4}r^2\left[\frac{\Delta\theta(V + V_o)}{\Delta z}\right]^2 = \frac{1}{4}r^2\,\frac{\Delta\theta^2}{\Delta z^2}(V^2 + V_o^2 + 2VV_o) \tag{15}$$

Make, for simplicity

$A = r^2\,\frac{\Delta\theta^2}{\Delta z^2}$, so

$$\frac{C_p p_o}{R\rho_o V_o}V + \frac{C_p V_o^2 \rho_o}{R\rho_o V_o}V - \frac{C_p V_o \rho_o}{R\rho_o V_o}V^2 + \frac{1}{2}V^2 + \frac{1}{4}A(V^2 + V_o^2 + 2VV_o)$$

$$= C_p T_o + \frac{1}{2}V_o^2 \tag{16}$$

$$V\left[\frac{C_p p_o}{R\rho_o V_o} + \frac{C_p V_o}{R}\right] + V^2\left[\frac{1}{2} - \frac{C_p}{R}\right] + \frac{1}{4}AV^2 + \frac{1}{4}AV_o^2 + \frac{1}{2}AVV_o$$

$$= C_p T_o + \frac{1}{2}V_o^2 \tag{17}$$

Noting that

$$\frac{p_o}{\rho_o} = RT_o$$

then

$$V^2\left(\frac{1}{2} + \frac{1}{4}A - \frac{C_p}{R}\right) + V\left(\frac{C_pT_o}{V_o} + \frac{C_pV_o}{R} + \frac{1}{2}AV_o\right) + \left(\frac{1}{4}AV_o^2 - C_pT_o - \frac{1}{2}V_o^2\right) = 0 \quad (18)$$

which is a very simple quadratic equation of the type:

$$a_1V^2 + a_2V + a_3 = 0 \quad (19)$$

where

$$a_1 = \frac{1}{2} + A/4 - C_p/R$$

$$a_2 = C_pT_o/V_o + C_pV_o/R + AV_o/2$$

$$a_3 = AV_o^2/4 - C_pT_o - \frac{1}{2}V_o^2$$

This Equation 20 can be easily solved using the general solution:

$$\frac{-a_2 \pm \sqrt{a_2^2 - 4a_1a_3}}{2a_1} \quad (20)$$

For the actual solution of Equation 20, refer to Appendix G.

# CHAPTER III

## EQUIPMENT, METHODS AND EXPERIMENTAL FACILITIES

### I. THE NOZZLES

In this study the following nozzles were used:

1. A 3 cm diameter convergent nozzle which is shown on Figure 2 was used as basic reference.

2. A pair of dual convergent circular nozzles, with and without guide vanes, was also used. These nozzles have the same exhaust area as the single 3 cm circular nozzle.

These last two nozzles (2) will be called from now on, multitubes number one (MT1) and two (MT2), the centerline distances being the main difference between the two (as shown on Figure 3). To the multitube number one (MT1) different internal guide vanes were used to rotate (spin) the flow. The guide vanes are named (see Figure 4) by the way that they rotate (spin) the flow.

If facing the nozzle exits (of MT1), from the outside of it, the rotation (spin) induced to the flow is clockwise then a positive rotation is achieved. A negative rotation is obtained by having guide vanes which spin the flow counterclockwise.

An example for a guide vane is a +30-30 meaning that facing MT1 from the outside, the left nozzle induces a 30 degree of positive (clockwise) spin to the flow and the

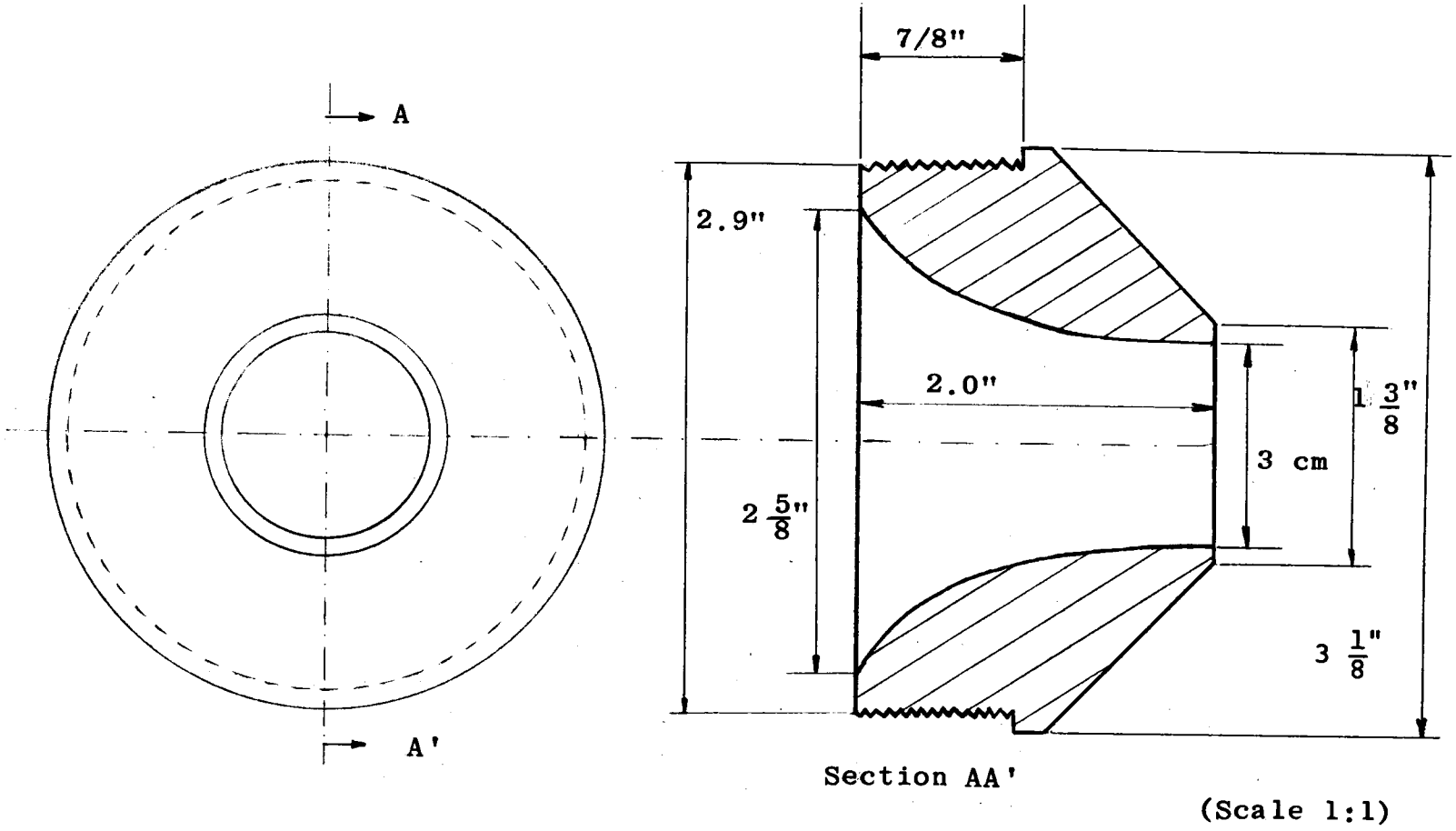


Figure 2. Three centimeter circular nozzle.

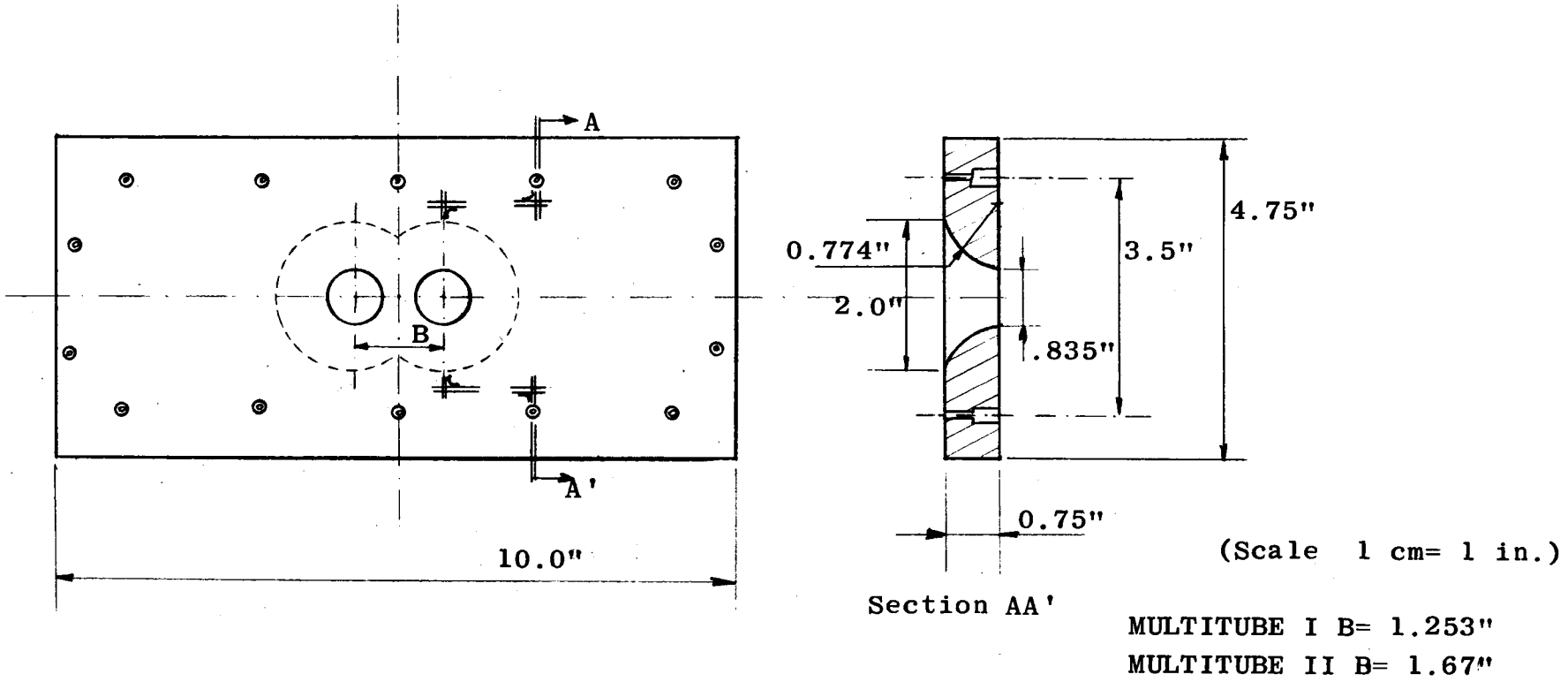


Figure 3. Multitube nozzles I and II, with equivalent exhaust area as a three centimeter circular nozzle.

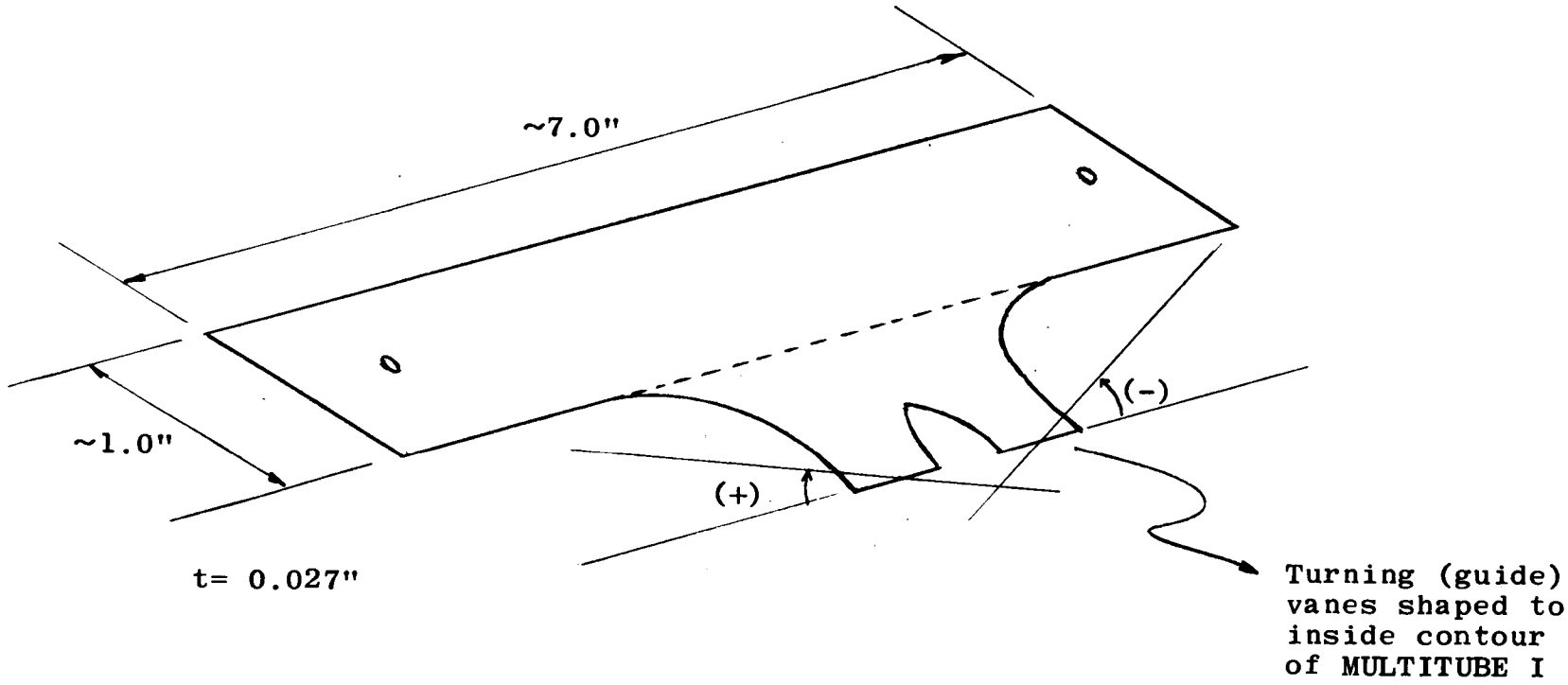


Figure 4. Zero degree turning (guide) vanes, also showing the (+) plus and (-) minus deflections of the vanes.

right nozzle induces a 30 degree of negative (counter-clockwise) spin to the flow as illustrated below.

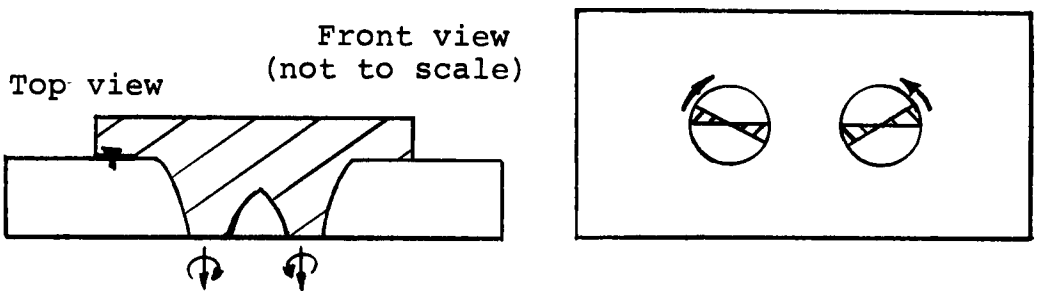


Several guide vanes were used in this investigation. They are as follows:

1. 0° (flat plate only)
2. +15-15
3. +30-30
4. +45-45
5. -15-15
6. +30+30
7. +45+45

Note that the same multiple mixing interference can be obtained by either having a +30-30 guide vane or a -30+30. Similar reasoning can be used for a +30+30 and a -30-30 configuration.

All these vanes were mounted on MT1 using two small screws and quick setting glue which made interchanging the vanes a minor task.

Both multitube nozzles could be attached to an

adaptor plate (shown on Figure 5). This adaptor plate, in turn, fitted both the reverberation room and free-field stilling chambers.

The 3 cm circular nozzle has also an adaptor plate which fits both stilling chambers (Figure 6).

Both multitubes and the 3 cm circular nozzle have been previously used by other investigators at The University of Tennessee Space Institute (5, 6, 7).

## II. REVERBERATION ROOM AND REVERBERATION TIMES

In order to evaluate the total sound power of the different jets, a reverberation room was used (Figure 7).

After a large number of successive reflections the sound, in the reverberation room, may be assumed to become diffuse (i.e., the average energy density is then the same throughout the room). A microphone placed in this diffuse field will give all the information on the total sound output of the jet.

This is, however, an oversimplified approach to the actual behavior of the sound waves in a room (particularly at low frequencies) because it neglects entirely such factors as the normal modes of vibration of the room, interference, diffraction, focusing effects, etc. (4).

The normal modes of vibration in a simple geometrical configuration (a rectangular chamber) such as the reverberation room can be easily calculated using a simple formula from Reference (4):

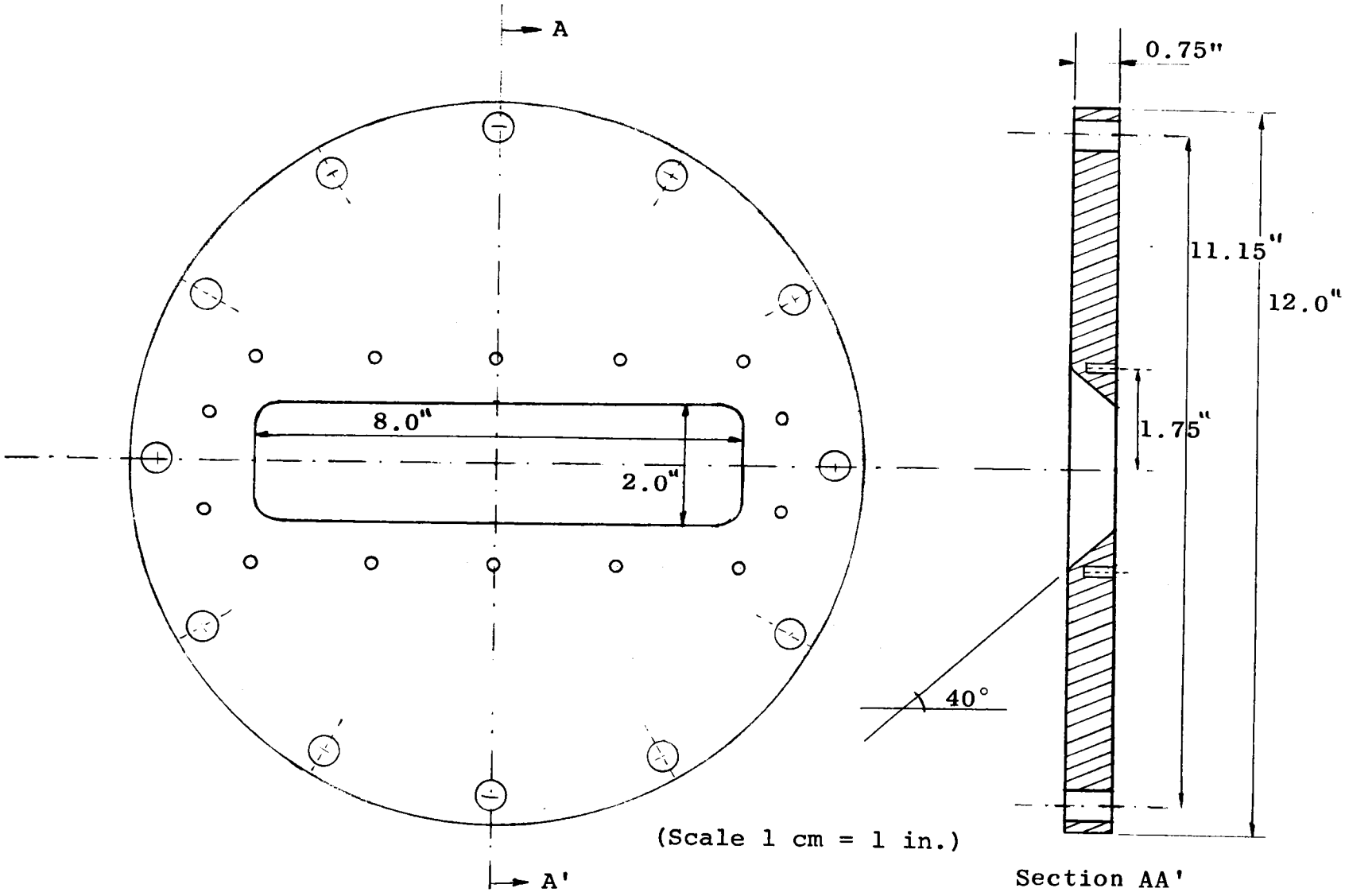


Figure 5. Multitube adaptor plate.

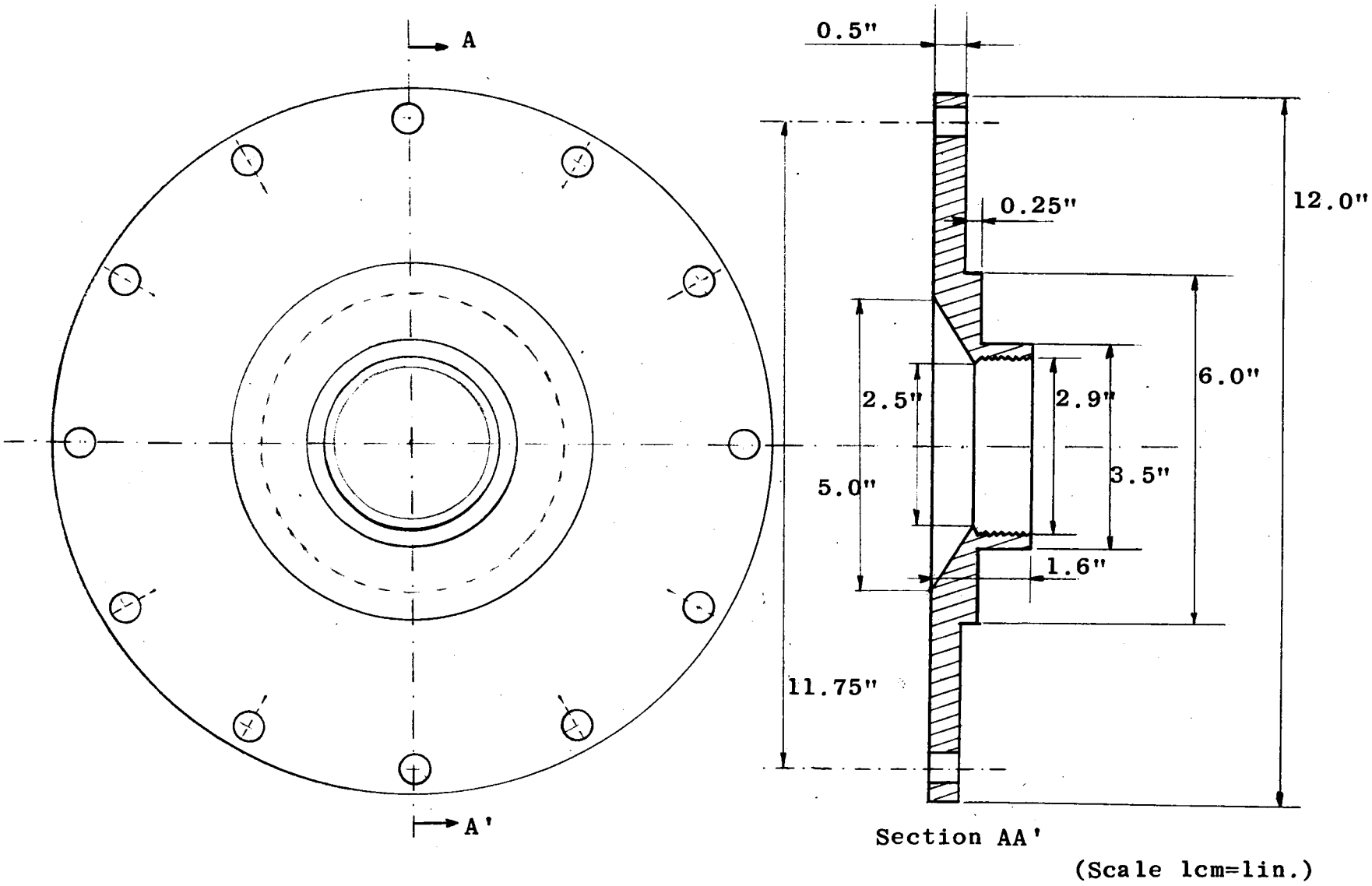


Figure 6. Three centimeter circular nozzle adaptor.

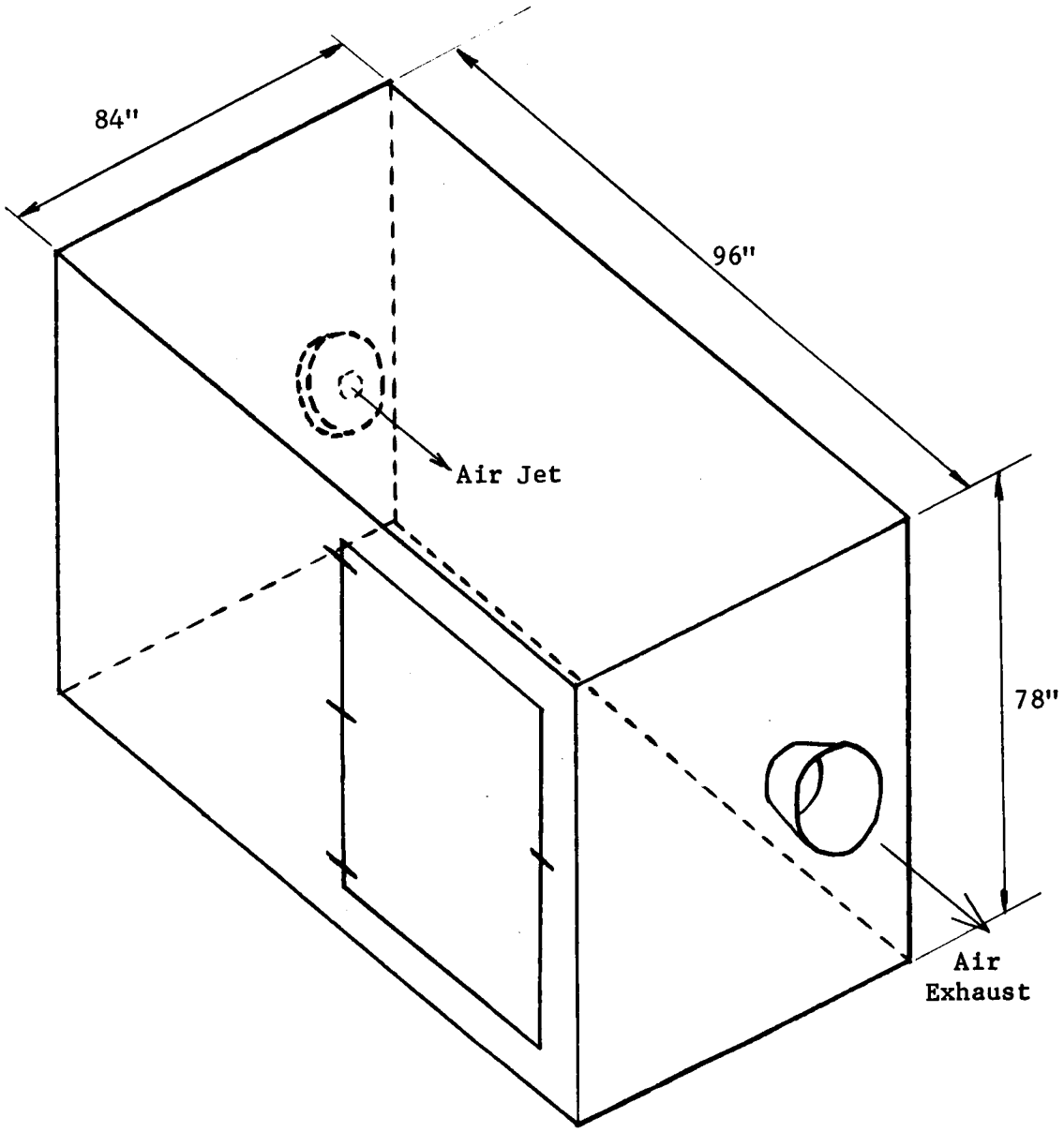


Figure 7. Reverberation room (schematically).

$$f = \frac{\omega}{2\pi} = \frac{c}{2}[(n_x/l_x)^2 + (n_y/l_y)^2 + (n_z/l_z)^2]^{1/2}$$

where c = 1100 ft/sec, and for the reverberation room used in these experiments:

$l_x$ = 84" = 7 ft

$l_y$ = 96" = 8 ft

$l_z$ = 78" = 6.5 ft

The lowest characteristic frequency for this room will occur when:

$n_x$ = 0

$n_y$ = 1

$n_z$ = 0, yielding

$f_{0,1,0}$ = 68.75 Hz

A room (i.e., the reverberation room) will act as a resonator and will respond strongly to those impressed sounds having frequencies in the immediate vicinity of any of its characteristic frequencies. Those frequencies are tabulated in Table I for the reverberation room up to 250 Hz.

This reverberation room has been used by other investigators (5, 6, 7). Harper (7) found the lowest frequency that could be reliably measured, in the room, to be of the order of 500 Hz.

We can, however, extrapolate this value down to about 250 Hz since as we get into characteristic frequencies (in the reverberation room) between 250 to 500 Hz the resonant

TABLE I

CHARACTERISTIC FREQUENCIES OF THE REVERBERATION ROOM UP TO 250 HERTZ

| Modes of the Room | | | Frequency (Hz) |
|---|---|---|---|
| $n_x$ | $n_y$ | $n_z$ | f |
| 0 | 1 | 0 | 68.7 |
| 1 | 0 | 0 | 78.5 |
| 0 | 0 | 1 | 84.6 |
| 1 | 1 | 0 | 104.4 |
| 0 | 1 | 1 | 109.0 |
| 1 | 0 | 1 | 115.4 |
| 1 | 1 | 1 | 134.3 |
| 0 | 2 | 0 | 137.5 |
| 2 | 0 | 0 | 157.1 |
| 1 | 2 | 0 | 158.3 |
| 0 | 2 | 1 | 161.4 |
| 0 | 0 | 2 | 169.2 |
| 2 | 1 | 0 | 171.5 |
| 2 | 0 | 1 | 178.4 |
| 1 | 2 | 1 | 179.5 |
| 0 | 1 | 2 | 182.6 |
| 1 | 0 | 2 | 186.5 |
| 2 | 1 | 1 | 191.2 |
| 1 | 1 | 2 | 198.8 |
| 0 | 3 | 0 | 206.2 |
| 2 | 2 | 0 | 208.8 |
| 0 | 2 | 2 | 218.0 |
| 1 | 3 | 0 | 220.7 |
| 0 | 3 | 1 | 222.9 |
| 2 | 2 | 1 | 225.2 |
| 2 | 0 | 2 | 230.9 |
| 1 | 2 | 2 | 231.7 |
| 3 | 0 | 0 | 235.7 |
| 1 | 3 | 1 | 236.3 |
| 2 | 1 | 2 | 240.9 |
| 3 | 1 | 0 | 245.5 |
| 3 | 0 | 1 | 250.0 |

peaks begin to overlap (see again Table I) and eventually the overall response curve will become relatively smooth.

The pressure amplitudes of all patterns of standing waves in a rectangular enclosure are at a maximum in the corners of the room. This was not quite the case with the air jets in question since the nozzles were mounted close to one of the edges of the room (not too far from one of the room corners).

Also, a microphone placed near the corner of a room will measure the peak sound pressure for every mode of vibration excited. In order to avoid this condition, several tests were conducted until two representative positions for the microphones (away from the corners, the walls and the jet) were found.

It can be shown (7) that by measuring the RMS pressure level of the sound (SPL, dB) and reverberation time (t, seconds) of a reverberation room, for any frequency band in question, the radiated sound power of the noise source (in that frequency band) can be determined.

The reverberation time, one of the easiest characteristics to be determined in a room, is defined (according to References (8, 9)) as the length of time (t) it takes the mean energy of a wave to reduce to a millionth ($10^{-6}$, i.e., 60 dB) part of its initial value.

To measure the reverberation time, the reverberation room was acoustically either excited by a .32 caliber blank pistol or a narrow band noise produced through a loudspeaker.

The signals were picked up by a single microphone, filtered and recorded on a chart, where dB of decay versus time was readily accessible (in any desired 1/3 octave frequency band, see Figure 8). For the reverberation times equipment set-up refer to Figure 9.

The reverberation times curve, for the reverberation room, is shown on Figure 10.

All data taken in the reverberation room were automatically corrected (in a data reduction computer program) for the reverberation times.

The reverberation room used is made of heavily reenforced plywood and it has the dimensions of 84" x 96" x 78". This room has a volume of about 364 $ft^3$ (10.3 $m^3$). The test nozzles were mounted inside the room where two microphones, placed at predetermined points in the diffuse field, pick up the sound signals.

The air is allowed to escape from this room through an 8" diameter opening to the outside (refer again to Figure 7, page 22).

The reverberation room stilling chamber is shown in Figure 11. It started first with a total length of 4 ft (48") but it has since been elongated twice (with two extension pieces) as a requirement for some tests. Figure 12 depicts its actual configuration. The nozzle adaptor plates previously mentioned could be bolted on straight to the end plate of the stilling chamber. This reverberation room has also been used by other investigators (5, 6, 7).

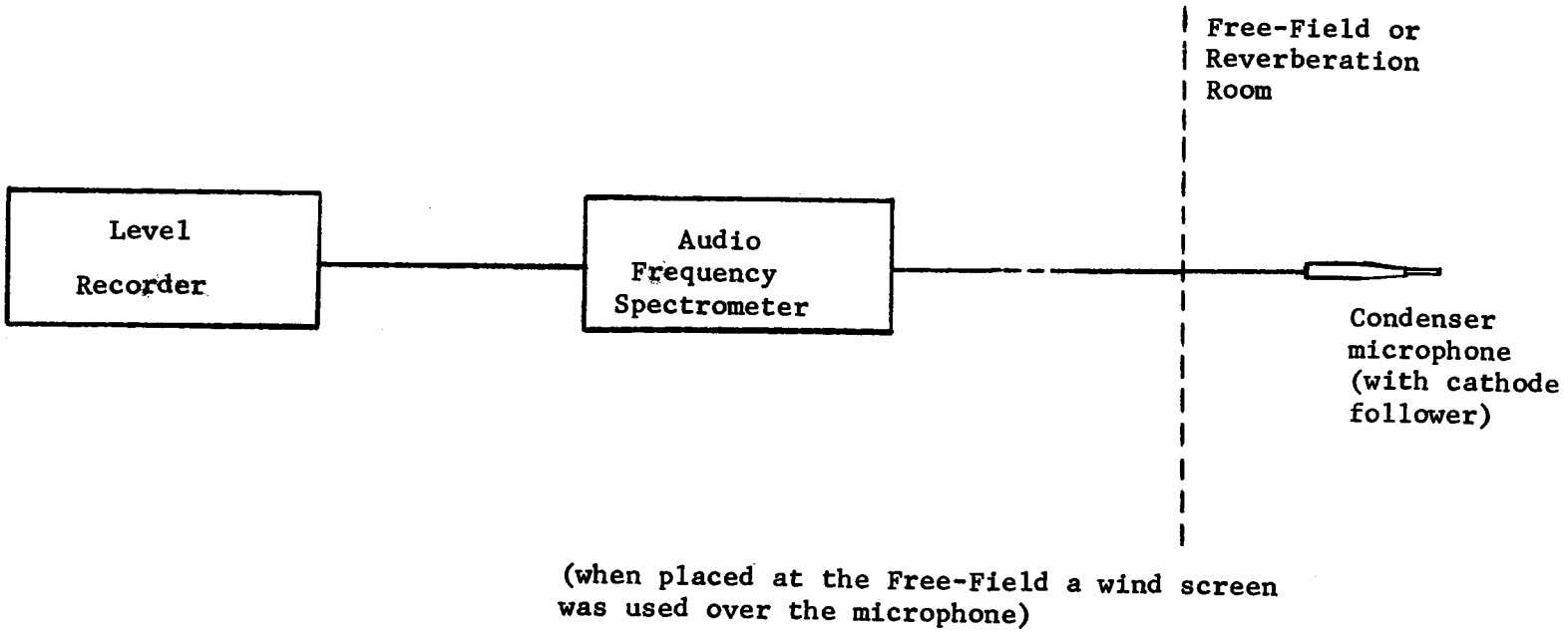


Figure 8. Basic sound recording equipment set-up.

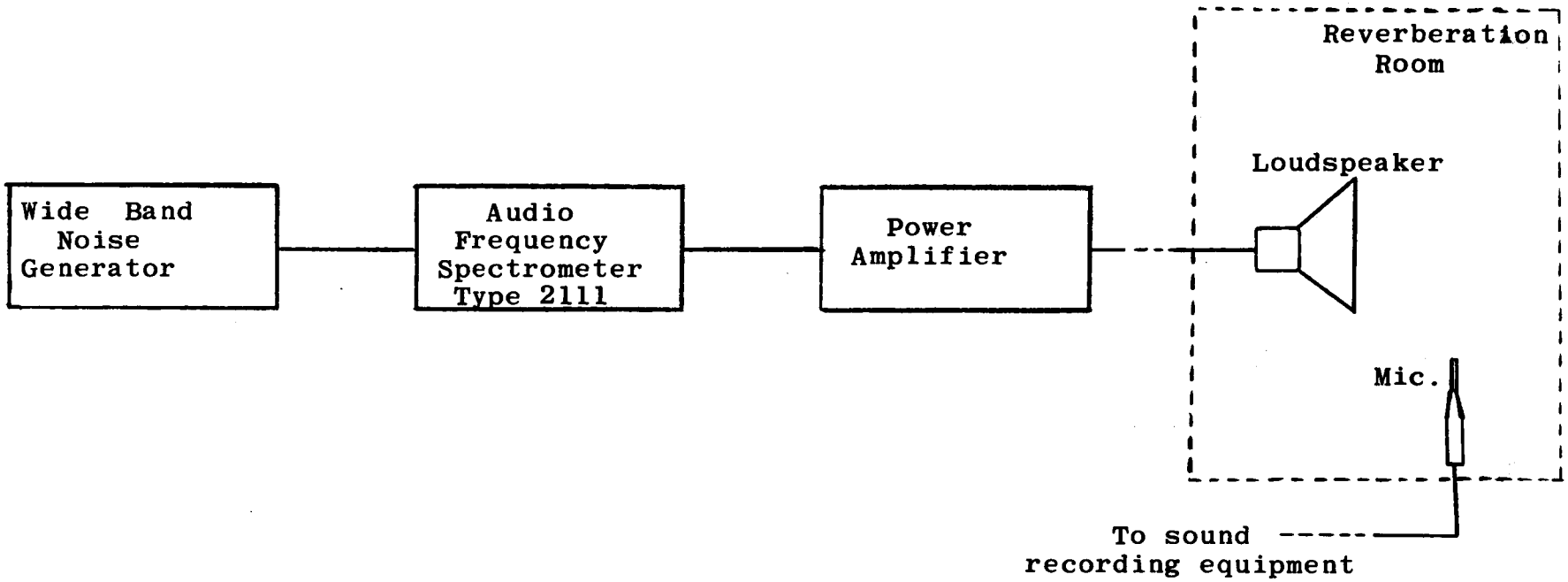


Figure 9. Reverberation times measurement set-up.

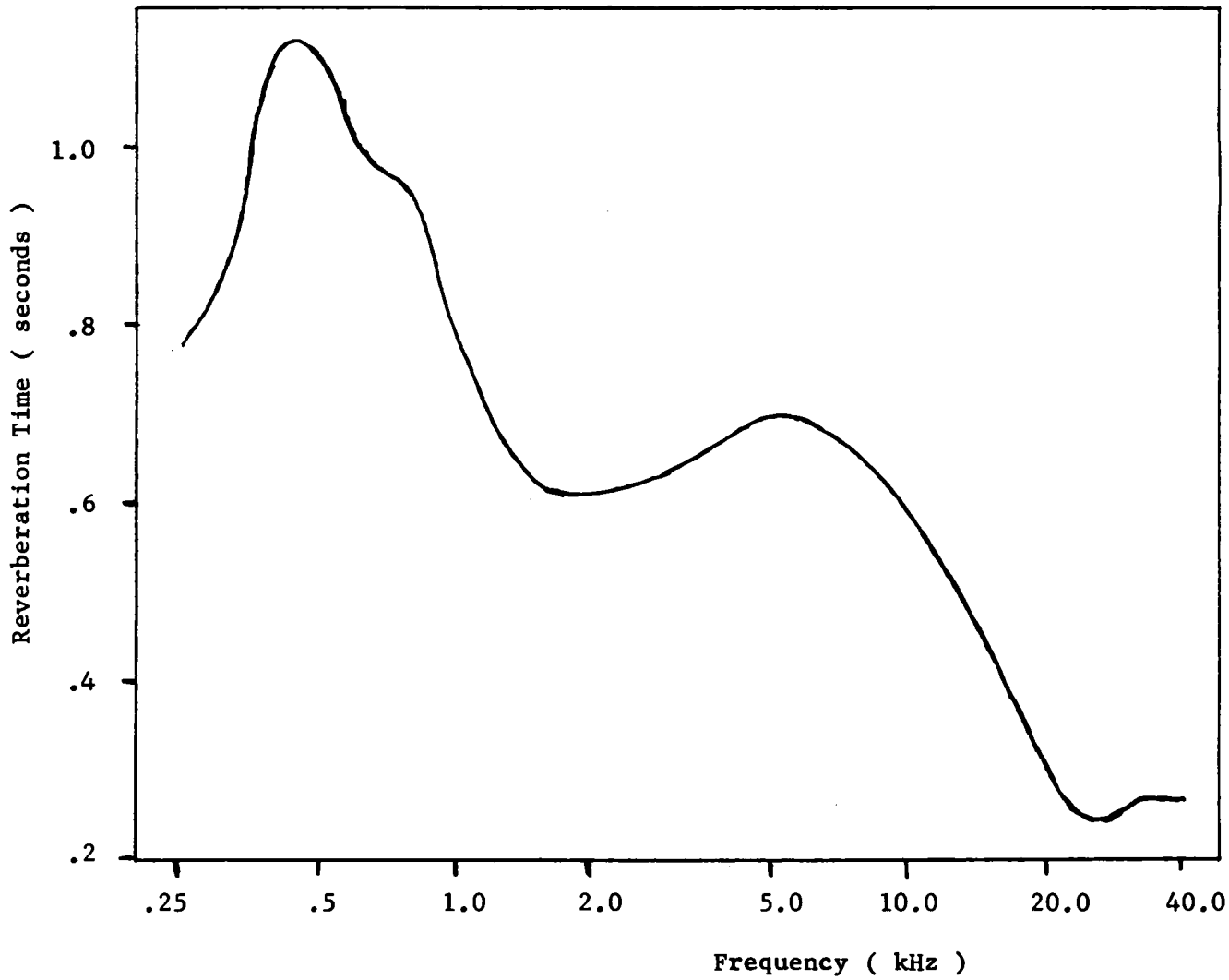


Figure 10. Reverberation times curve.

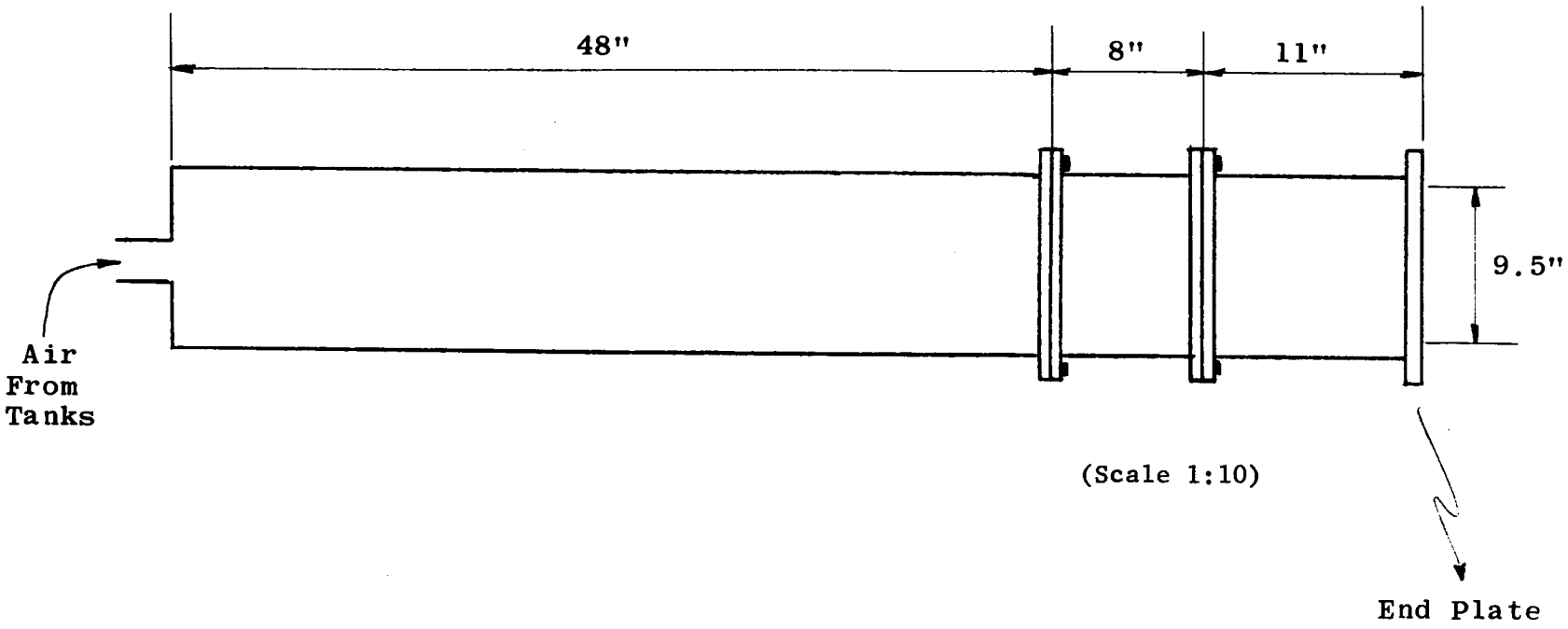


Figure 11. Reverberation room stilling chamber.

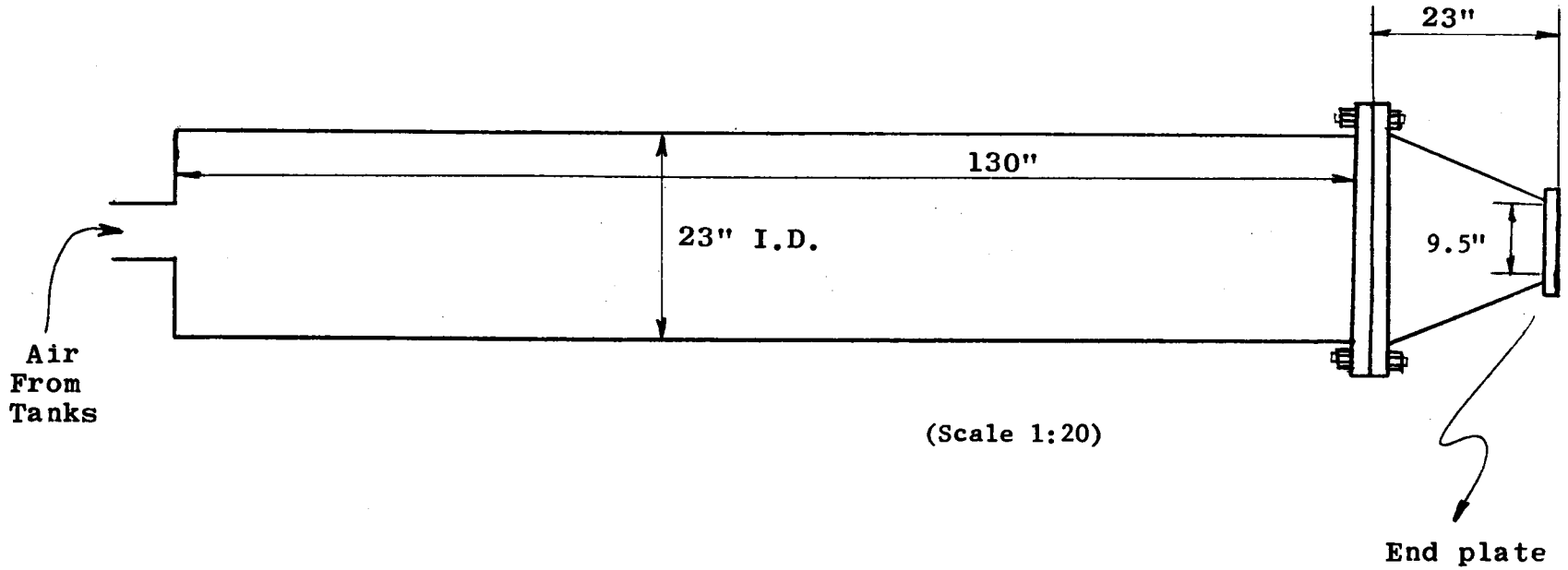


Figure 12. Free-field stilling chamber.

# III. THE FREE-FIELD

In order to assess the directional characteristics of the test nozzles, The University of Tennessee Space Institute free-field facility was used. It consists primarily of two systems (see Figures 13 and 14):

1. A large stilling chamber (Figure 14) which is mounted in such a way as to be able to be rotated from the horizontal position (parallel to the ground) to an angle of 35.5 degrees with the horizontal plane (as on Figure 13). With it horizontal it is relatively easy to exchange test nozzles. At an angle of 35.5 degrees free-field acoustic data were taken. The two nozzle adaptors previously described could be easily bolted onto the end plate of this stilling chamber.

2. A microphone sweep-arm which is driven by an electric motor mounted in its base, could be placed on three different concrete pods. From these three different positions, all nozzle planes of symmetry could be swept (Figure 14) by a microphone mounted at the end of the sweep-arm and at a radius of 13 ft from the nozzle exits. These arms could also be stopped at any point in the sweep (any angle) so that frequency spectra could also be obtained. A large protractor mounted around the sweep-arm would give its precise position in relation to the axis being swept.

An important step was to carefully isolate both electrically and mechanically the microphone from the

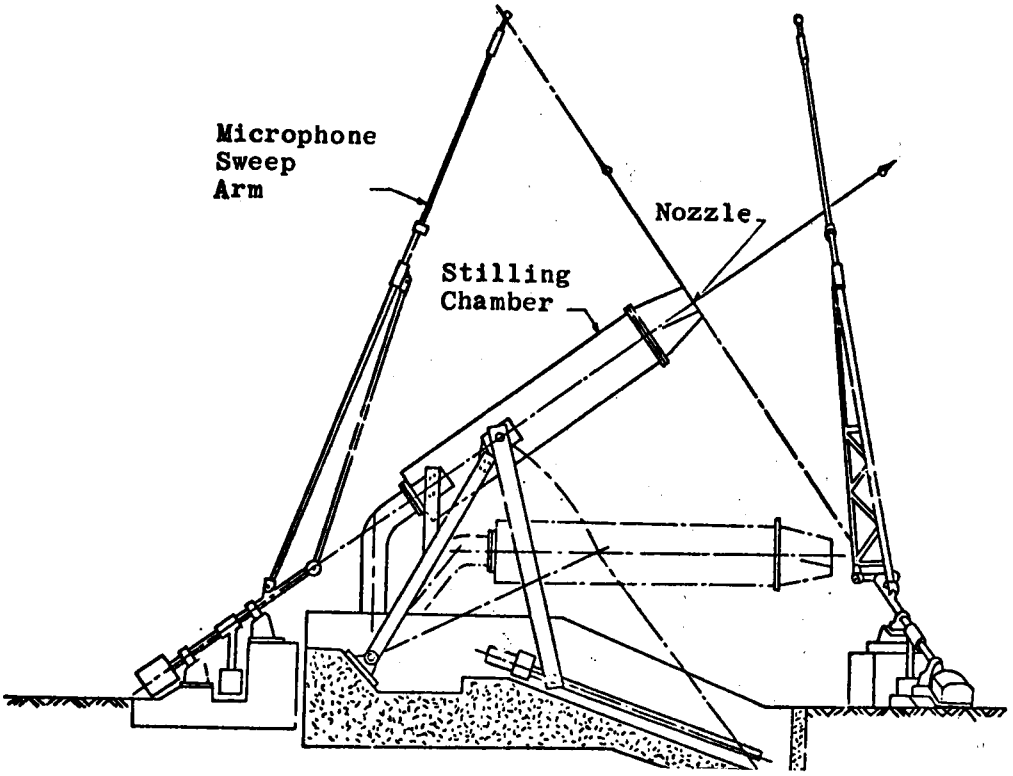


a) Elevation view

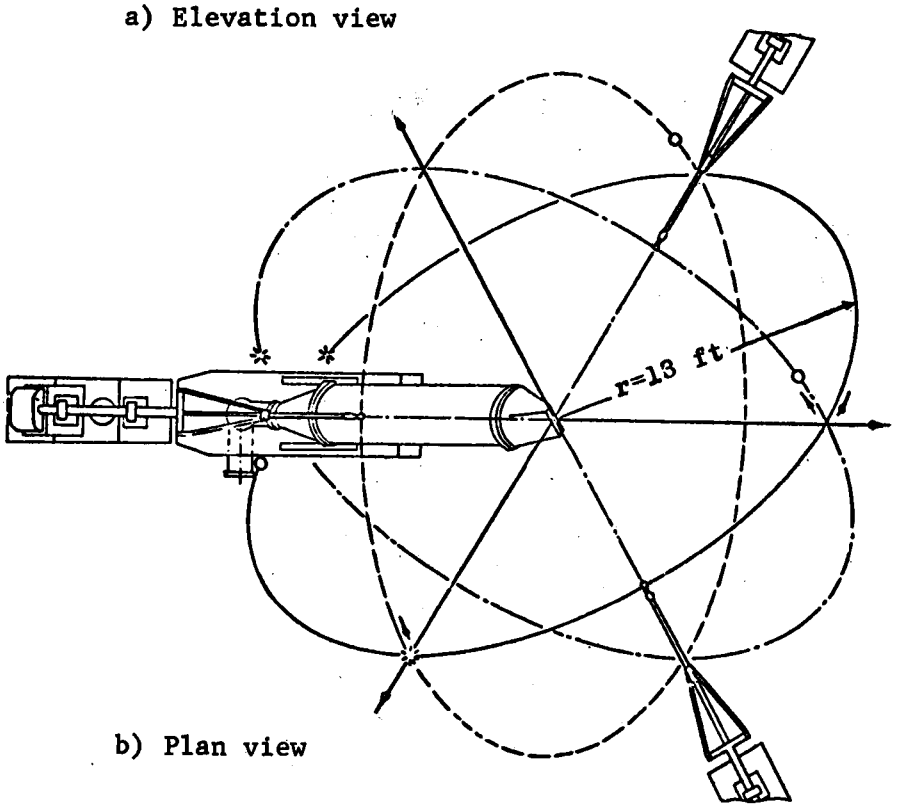


b) Plan view

Figure 13. Plan view of free-field facility.

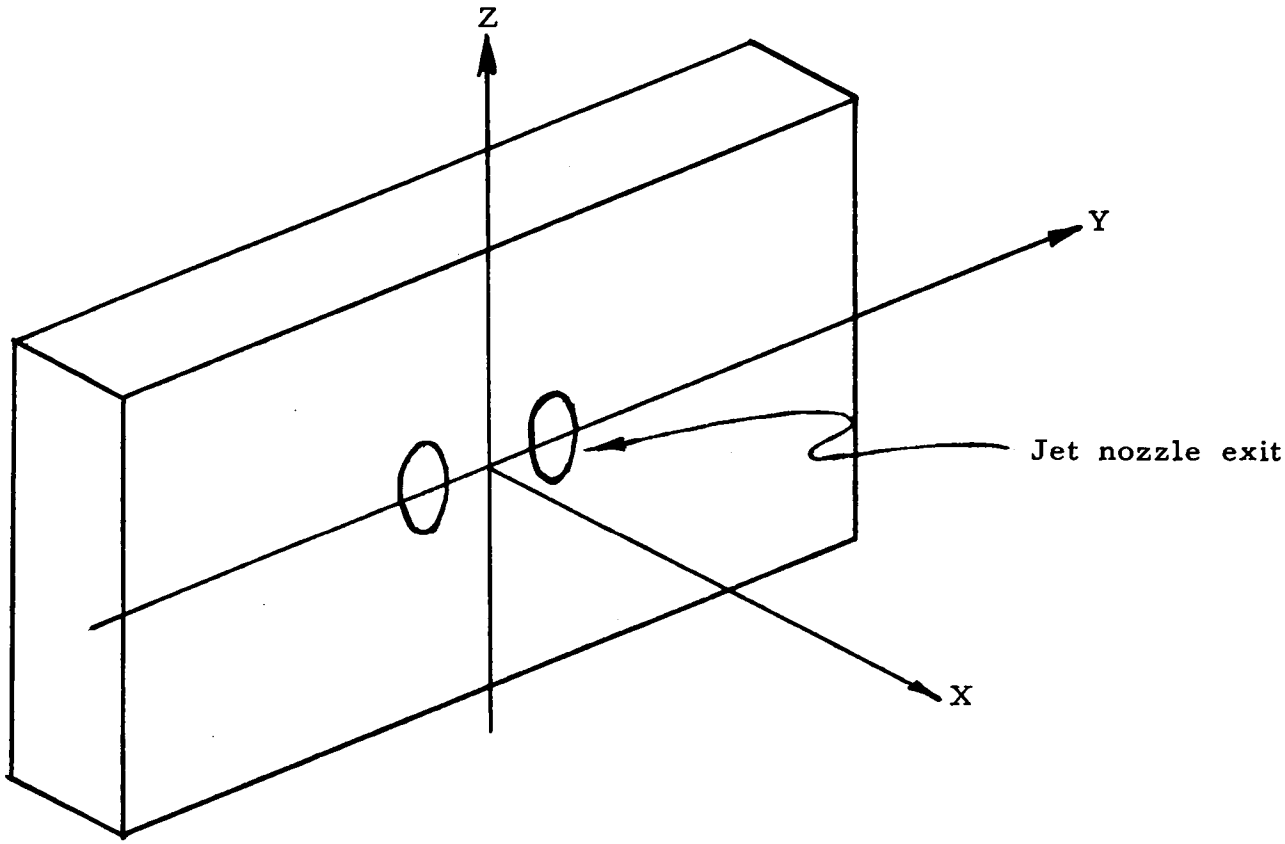


Figure 14. Principal planes of symmetry of multitube nozzles.

sweep-arm it was mounted to. The sweep-arm, which is about 20 ft long, would greatly amplify the mechanical vibrations of its drive motor. The isolation from this vibration was finally solved by mounting the microphone to an air balloon which dampened the sweep-arm vibrations.

## IV. AIR SUPPLY AND FLOW CONTROLS

The cold air supply system used in all of the experiments, consists of three 250 $ft^3$ tanks which could be pressurized to a maximum of about 3200 psig, by several air compressors.

From these tanks, the air was piped to both stilling chambers (free-field and reverberation room). Only one of the two above chambers could be operated at one time. This system provided more than adequate air supply to the 3 cm circular nozzle and its equivalent exhaust area multitubes (MT1 and MT2).

Due to a much larger volume of the free-field stilling chamber (32.5 $ft^3$, over ten times larger than the reverberation room stilling chamber) it was easier to maintain a steady chamber pressure which would yield a constant velocity jet exhaust. The reverberation room stilling chamber pressure was not more difficult to obtain, it just required constant attention from the operator. The volume of this last chamber is just 2.75 $ft^3$.

Assuming linear velocity profiles, the average air velocity in the larger chamber is about 1.74 ft/sec and in

the smaller one it is close to 10.2 ft/sec, when the cold around 70 °F) air flow through the nozzle is about $M_e$ = 0.95.

Figure 15 shows the control board as seen by the operator. The air supply system is shown on Figure 16. This figure also shows the points, in the flow system, where various pressures and temperatures are monitored (refer again to Figure 15).

Several thermocouples were mounted at different points in the flow so that the temperatures could also be measured. Each stilling chamber had a thermocouple inside. There was also one inside the reverberation room and another in the venturi meter. These temperatures could easily be monitored from the control board by simply dialing the selector for the desired thermocouple (refer to Figure 17).

## V. ACOUSTIC INSTRUMENTATION

Two separate channels (I and II) were used to record the signals from the reverberation room. In the free-field channel I was employed since only one microphone could be used at one time. For detailed information on all test equipment used, refer to Appendix B.

To calibrate the systems, before each test, a piston-phone calibrator was used. It produces a sound level signal of 114 dB at various frequencies (the test frequency used, though, was 1000 Hz).

All the frequency spectra generated were obtained

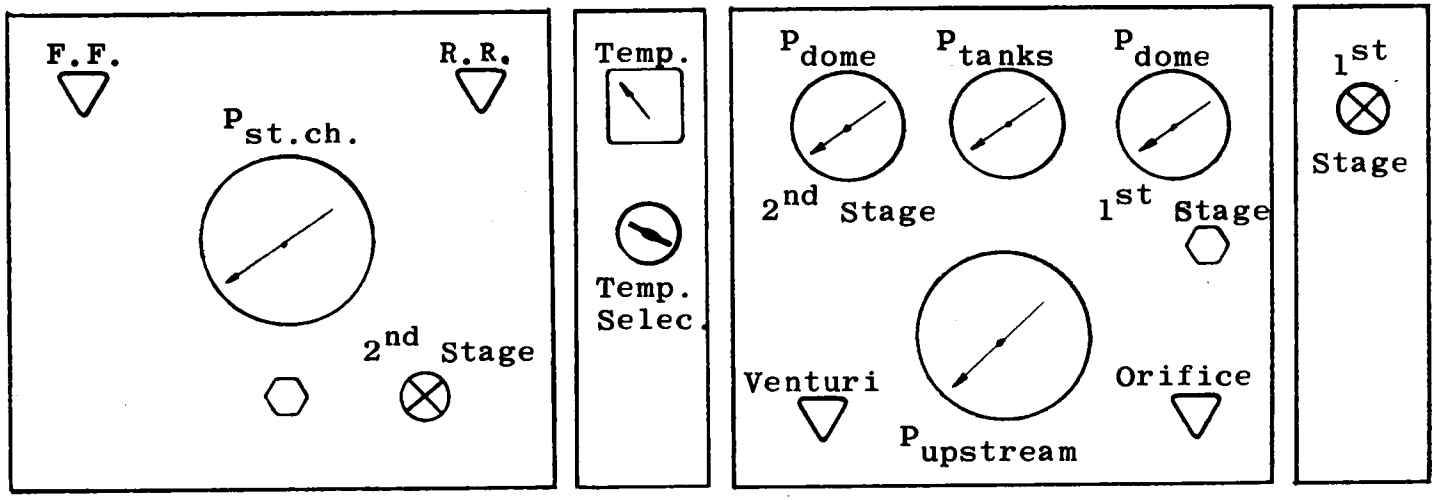


(also some U-tube manometers)

Symbols and abbreviatons:

F.F.- Free Field

R.R.- Reverberation Chamber

- Vents

- Hand Operated Valves

- Pressure Regulators

Figure 15. Control board.

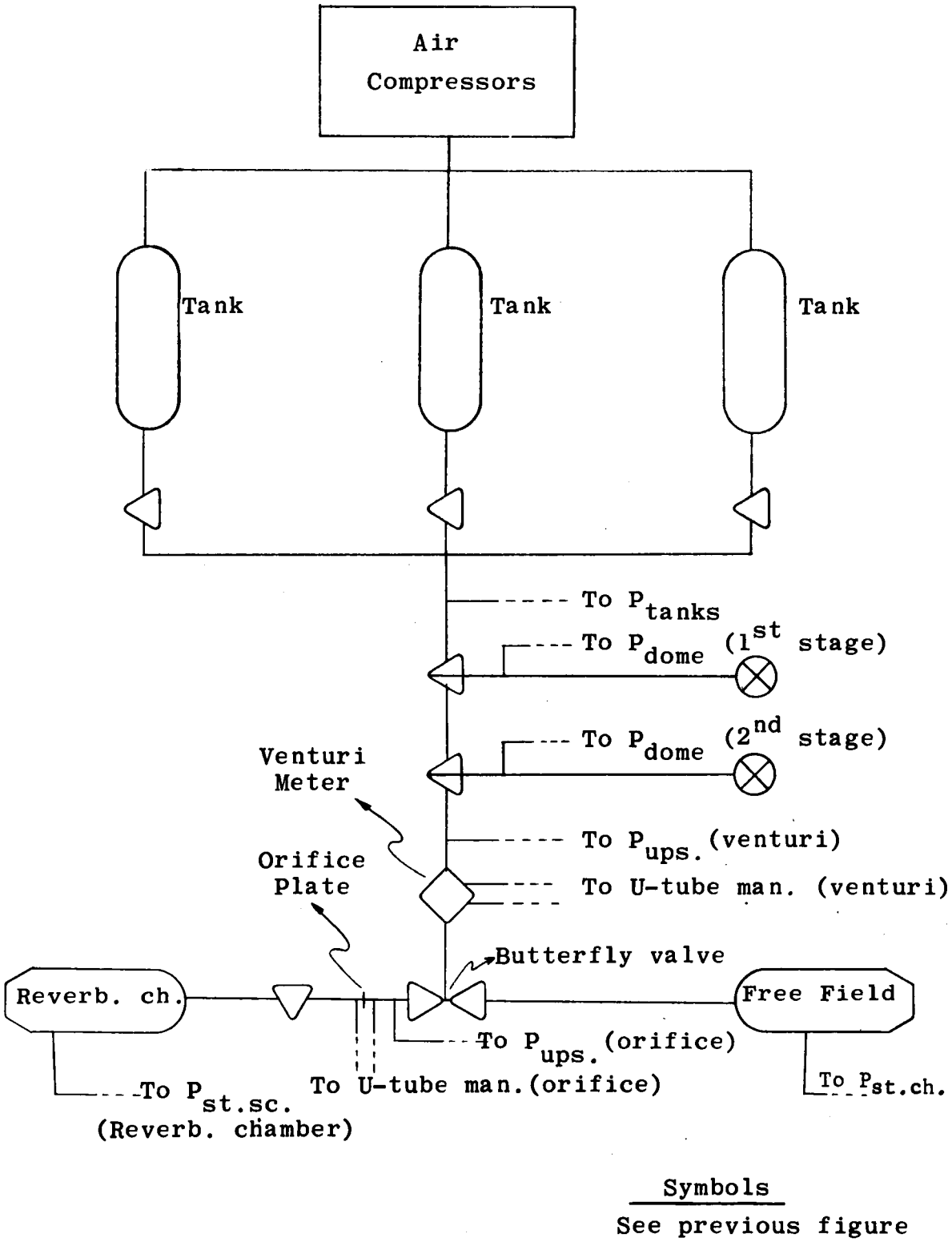


Figure 16. Air supply system.

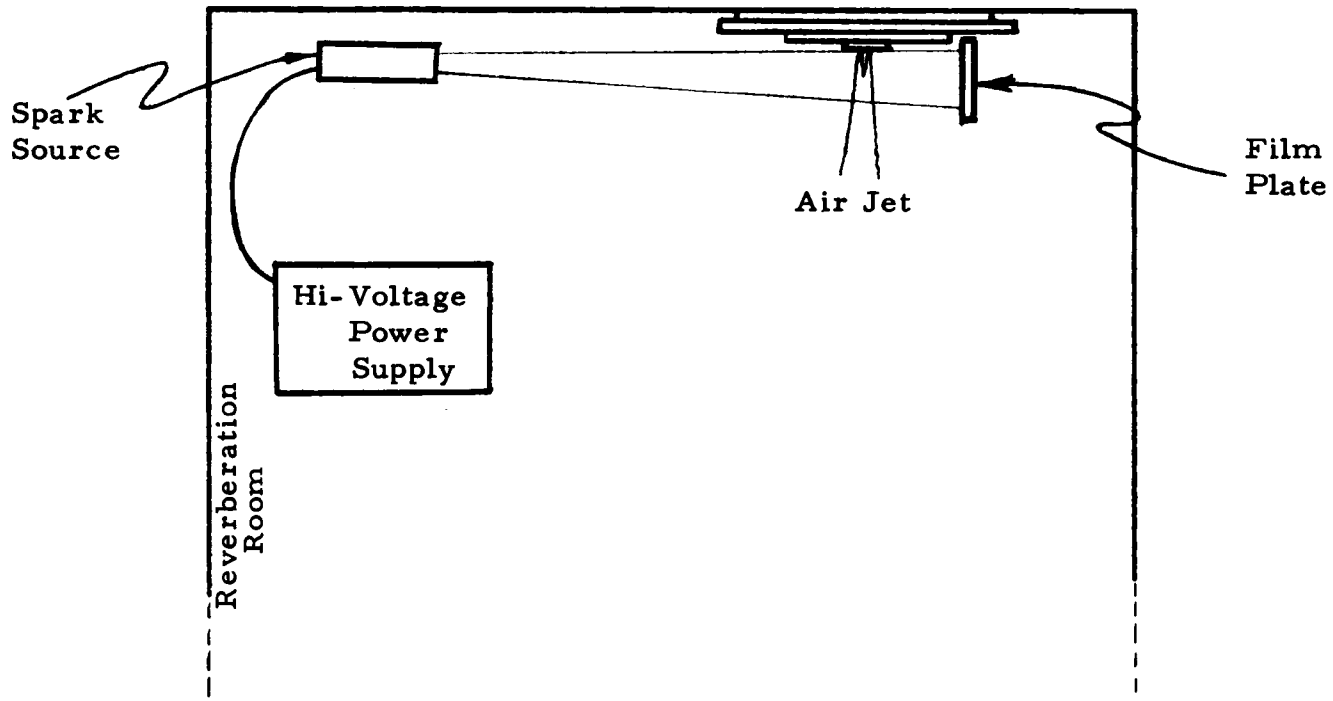


Figure 17. Shadowgraph equipment (schematically).

using a 1/3 octave spectrometer. The 1/3 octave center frequencies and bandwidths are given on Table II.

As outlined before, the reverberation times of the reverberation room were investigated. The acoustic signals were always filtered and recorded through channel I (see Figure 8, page 27). Two different methods were used:

1. By using a blank cartridge .32 caliber pistol.

2. Using a wide band noise which was filtered to a narrow band by using the audio frequency spectrometer type 2111 and then amplified and reproduced through a loudspeaker.

The difference, in these two methods of reverberation times measurement, lies only in the way that the acoustic waves were excited in the reverberation room (either using the pistol or the narrow band as noise generators). The pistol was used at very high frequencies since the loudspeaker cannot reproduce, properly, frequencies of 20 kHz and above.

## VI. THE SHADOWGRAPH METHOD

Shadowgraph flow photographs were also taken, inside the reverberation chamber, in order to better understand the flow field around multiple jets with and without swirling flow.

The shadow method allows for visual observation of density gradients in a flow field (10). The dark and bright spots in the shadowgraph correspond to maximum and minimum values, respectively, of the second derivative of the density.

TABLE II

ONE-THIRD OCTAVE BANDWIDTH CENTER FREQUENCIES

| Center Frequency (Hz) | 3 dB Bandwidth (Hz) |
|---|---|
| 250 | 58 |
| 315 | 73 |
| 400 | 92 |
| 500 | 116 |
| 630 | 145 |
| 800 | 183 |
| 1,000 | 230 |
| 1,250 | 290 |
| 1,600 | 370 |
| 2,000 | 460 |
| 2,500 | 580 |
| 3,150 | 730 |
| 4,000 | 920 |
| 5,000 | 1,160 |
| 6,300 | 1,450 |
| 8,000 | 1,830 |
| 10,000 | 2,300 |
| 12,500 | 2,900 |
| 16,000 | 3,700 |
| 20,000 | 4,600 |
| 25,000 | 5,800 |
| 31,500 | 7,300 |
| 40,000 | 9,200 |

This can clearly show the air flow pattern of a jet exhaust. Figure 17, page 39, shows the schematics of the equipment set-up.

The closeness of the film plate to the air jet bears a direct relationship to what will be made more clearly visible (13). If the film plate is placed relatively close to the air jet (6" or less) the turbulent structure will appear with good contrast. If, however, the film plate is placed at some distance to the jet (usually greater than 6") then the acoustic field will also be visible.

# CHAPTER IV

# DATA AND RESULTS

## I. INTRODUCTION

The data collected during this investigation consisted of the following:

1. Acoustic data: Overall sound pressure levels (OASPL, dB) and frequency spectra curves (SPL, dB) were the output of the acoustic equipment, both in the reverberation room and the free-field. From this, sound power levels (PWL, dB) can be easily computed as it was previously mentioned.

2. Flow data: By knowing the total and differential pressures and temperatures of the air flow at critical points, it was possible to compute, from one-dimensional isentropic gas dynamic relations, such parameters as the jet Mach numbers, exit velocities and mass flow rates.

3. Shadowgraphic data: Data which were taken in the reverberation room (and will be discussed together with other data from the reverberation room) helped to better understand the flow field around the nozzles.

Since the data referred to in 1 and 2 were taken both in the reverberation room and the free-field they will be introduced by that order (for a definition of the units used in this chapter, refer to Appendix A).

## II. REVERBERATION ROOM DATA

The MT1 nozzle showed a decrease of 1-2 dB (PWL) when compared with the circular nozzle (for a sample of all data collected refer to Appendices C and D). For the Mach number range of 0.5-0.9 this ΔPWL is larger at higher subsonic flows (see Figures 18, 19, and 20). The overall sound power data for the multitube nozzles with swirl is also shown in these figures. The overall sound power is, in general, higher for higher degrees of swirl. Note too, in these figures, that same sign spins means that both nozzles (of the twin multitubes only) have the same, positive or negative, spins as outlined in Chapter III. Similarly, different sign spins means that one of the nozzles has a positive spin and the other a negative one.

The sound power spectra of both MT1 and circular nozzles is shown on Figure 21 and shows the following trend: The circular nozzle is louder up to the mid-frequencies of about 8000 Hz. At the high end side of the spectra (above 10 kHz) the multitube nozzle is either slightly louder or at the same level as the circular nozzle.

The multitubes with swirl were found to be somewhat louder at very high frequencies probably due to the noise generated by the flat plate which produces the swirl. This was investigated by comparing the MT1 without vanes and the same multitube with a zero degree vane (flat plate) which does not introduce any swirl to the flow.

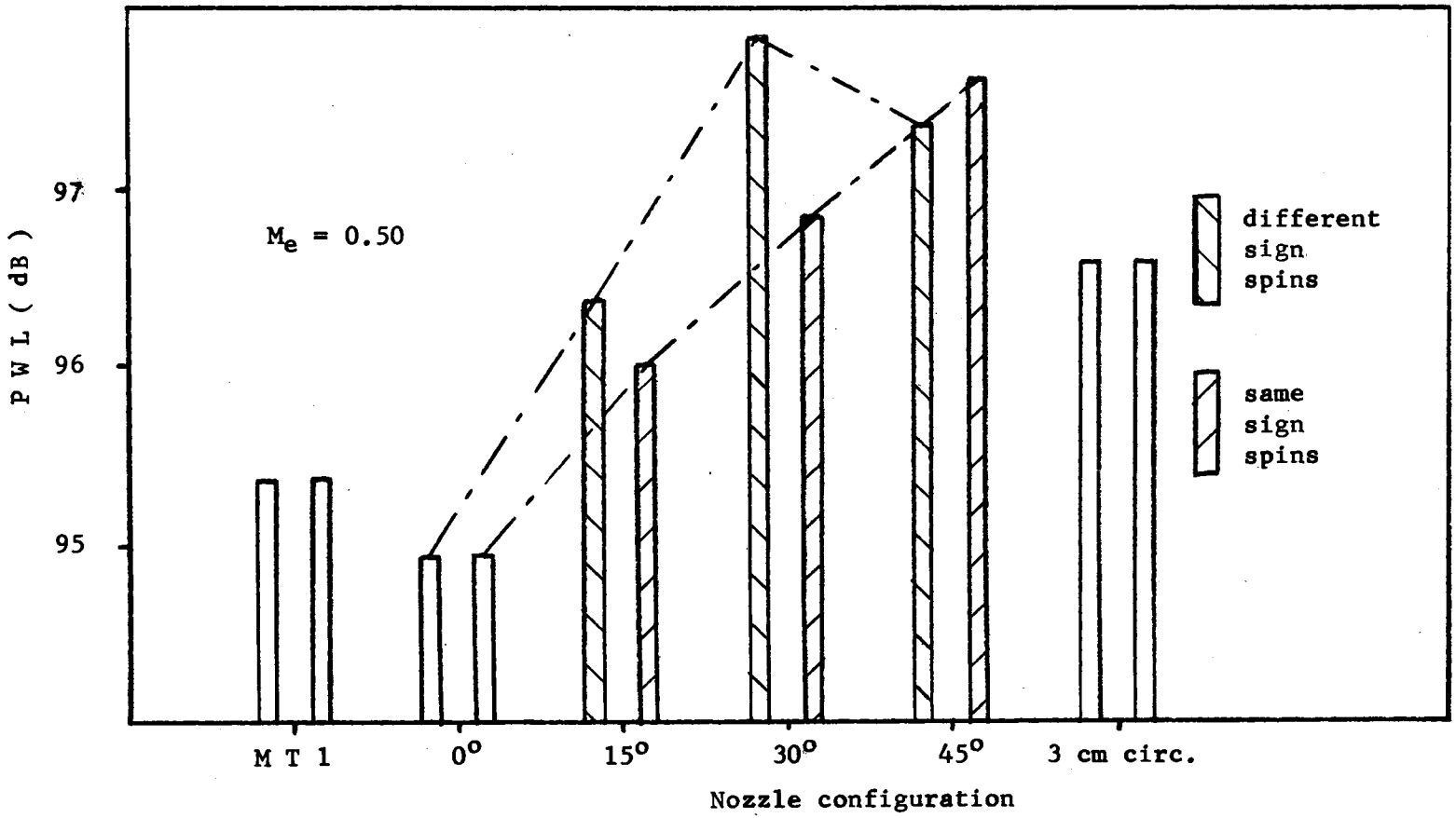


Figure 18. Overall sound power versus nozzle configuration at $M_e$ = 0.50.

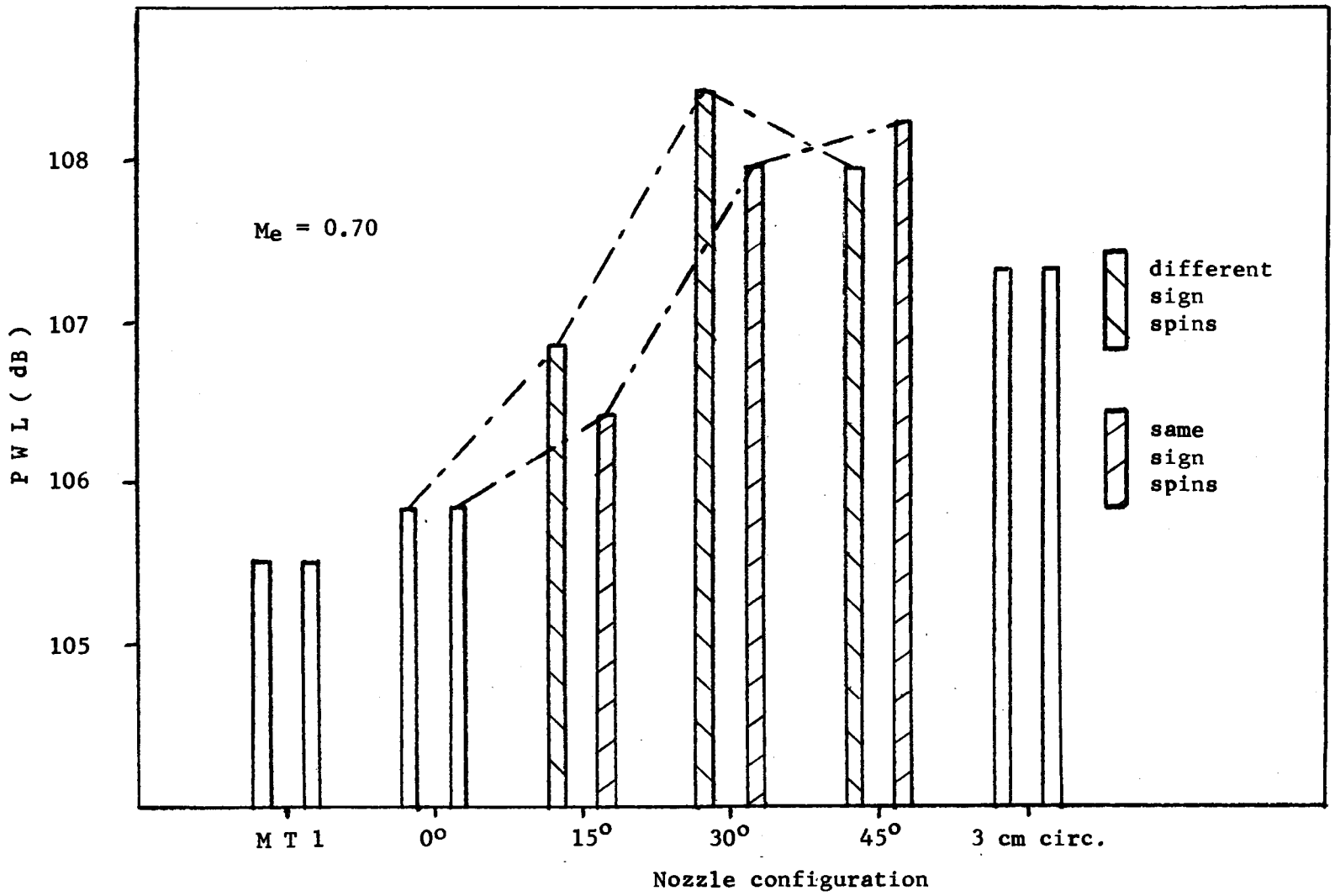


Figure 19. Overall sound power versus nozzle configuration at $M_e$ = 0.70.

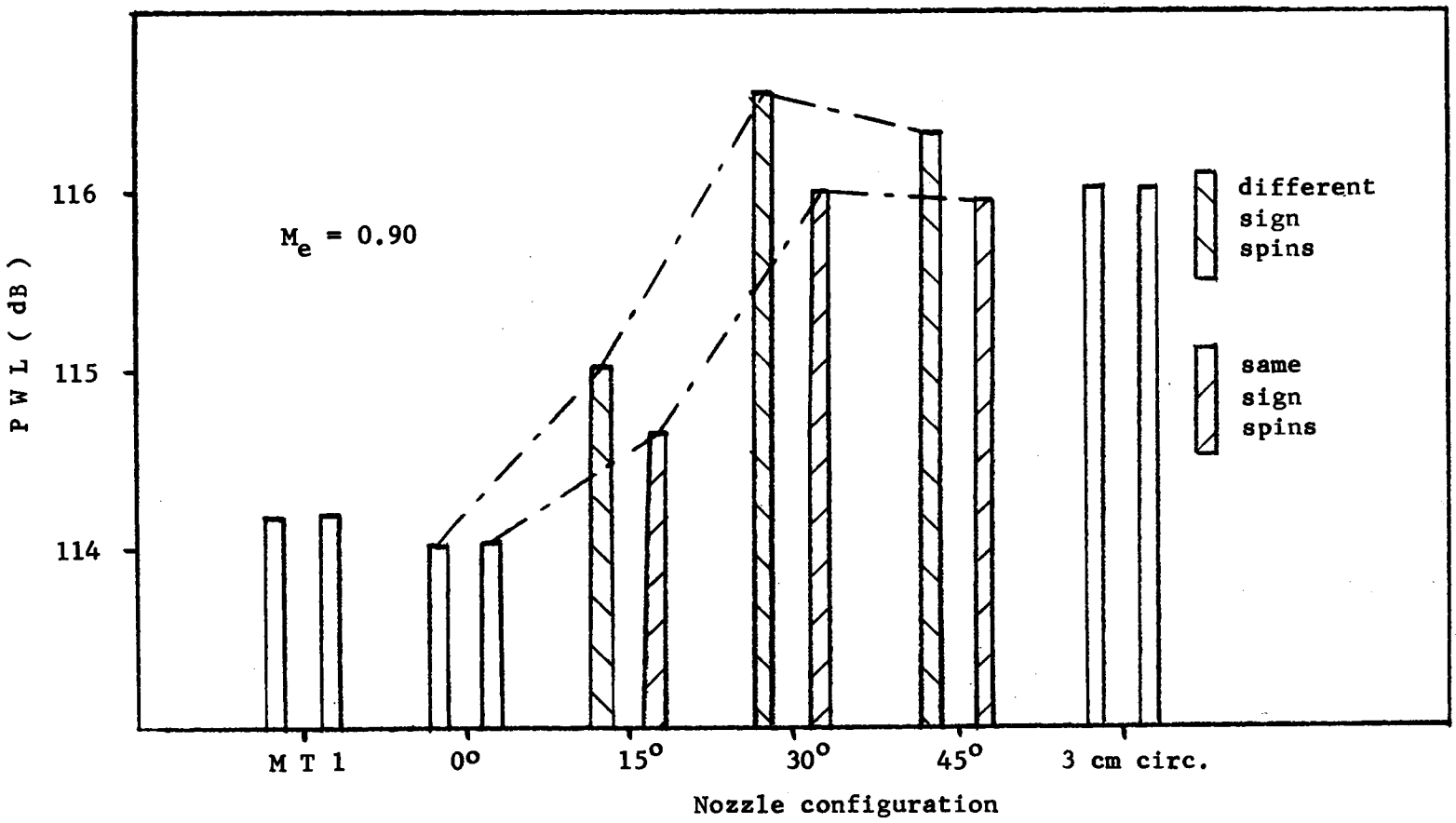


Figure 20. Overall sound power versus nozzle configuration at $M_e$ = 0.90.

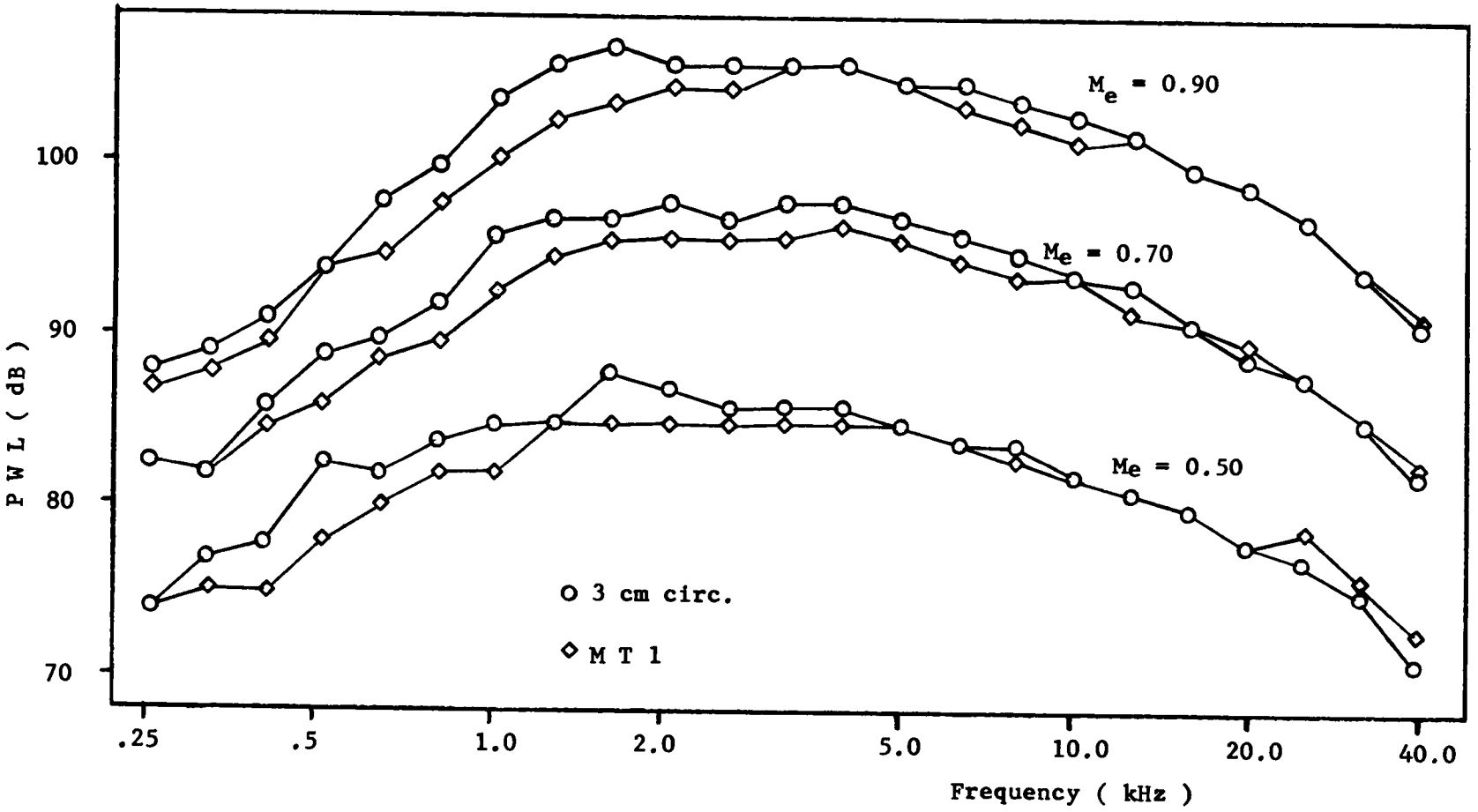


Figure 21. Frequency spectra at three different Mach numbers for the MT1 and the three centimeter circular nozzle.

The frequency spectra of the MT1 and the zero degree configuration are shown on Figure 22. It can be seen that both configurations are practically identical. If the guide vanes affect the sound generated by the jets, it will only be beyond the measured 40 kHz.

Figure 23 shows a very important point. The MT1 is definitely noisier at lower frequencies (below 3-4 kHz) and quieter above this value. It is very important to realize that this plot only shows the 45 degree swirls and the MT1 at Mach = 0.90 but both the 30 and 15 degree swirls also show the same trend at $M_e$ = 0.90, $M_e$ = 0.70 and $M_e$ = 0.50 as well. So Figure 23 is more general than it actually looks. The 45 degree case was used since it has the most "drastic" swirl. $M_e$ = 0.90 was chosen since it is the range mostly related with practical aircraft applications.

The next figures show even better the frequency shifts of the multitubes with swirl when compared with the more conventional MT1 and the 3 cm circular nozzles. The first two figures (Figures 24 and 25) show the spectra mean frequency ($f_{mean}$) plotted against Mach number. The $f_{mean}$ is defined as:

$$f_{mean} = \frac{\int fG(f)df}{P}, \text{ where}$$

$P = \int G(f)df$, total sound power, also

$dP = G(f)df$

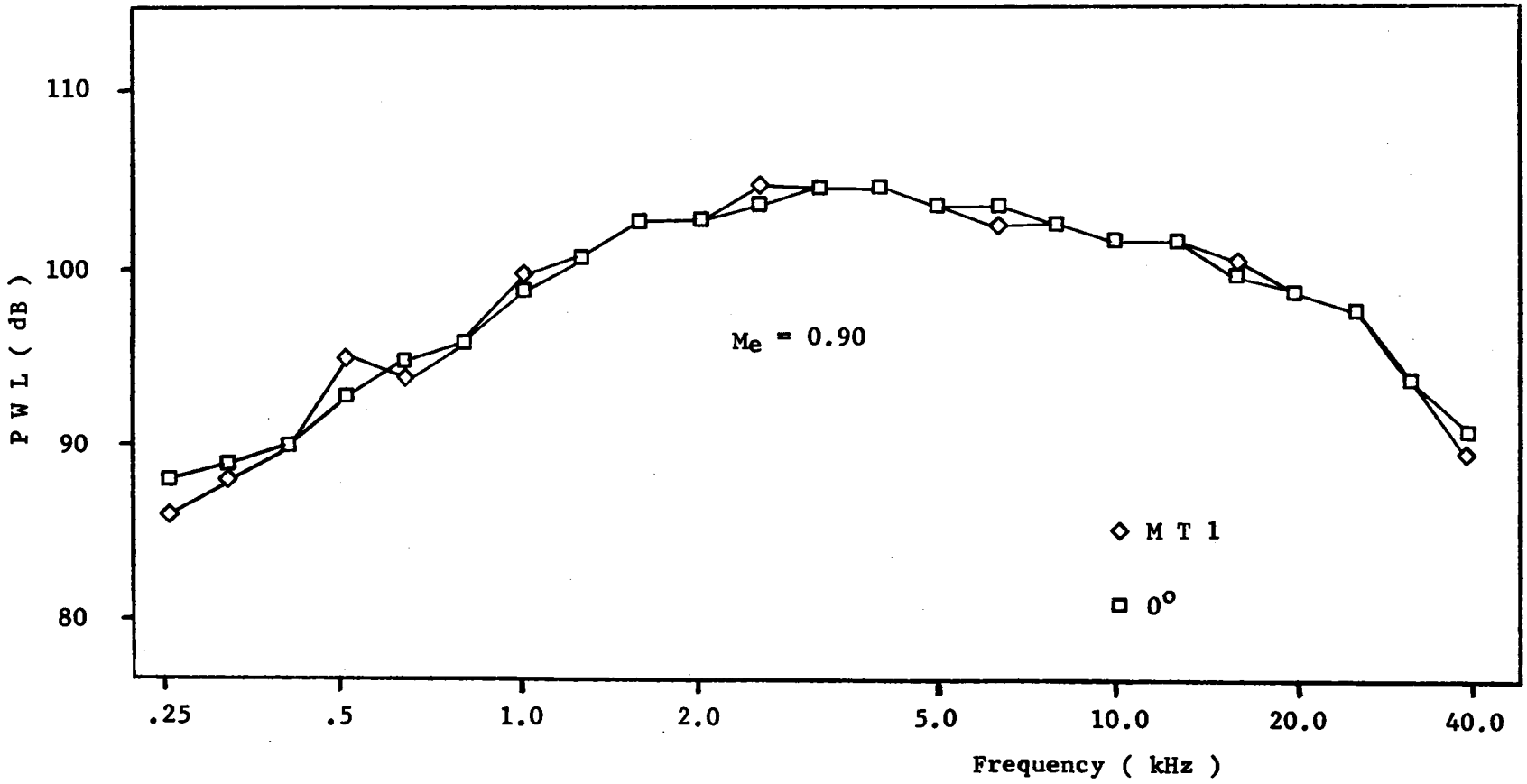


Figure 22. Frequency spectra of the MT1 and the zero degree guide vane nozzles.

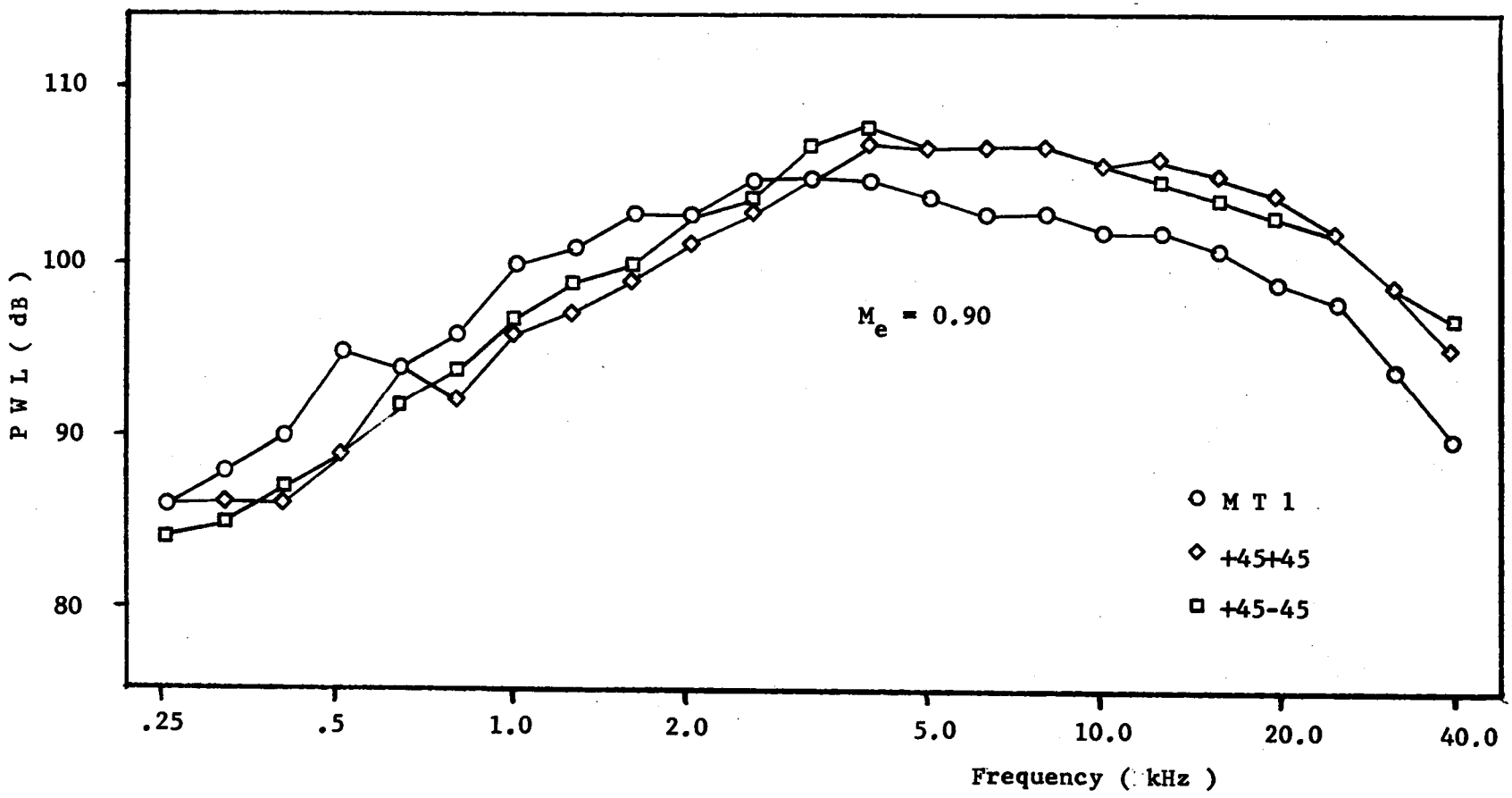


Figure 23. Sound power versus frequency for three nozzle configurations.

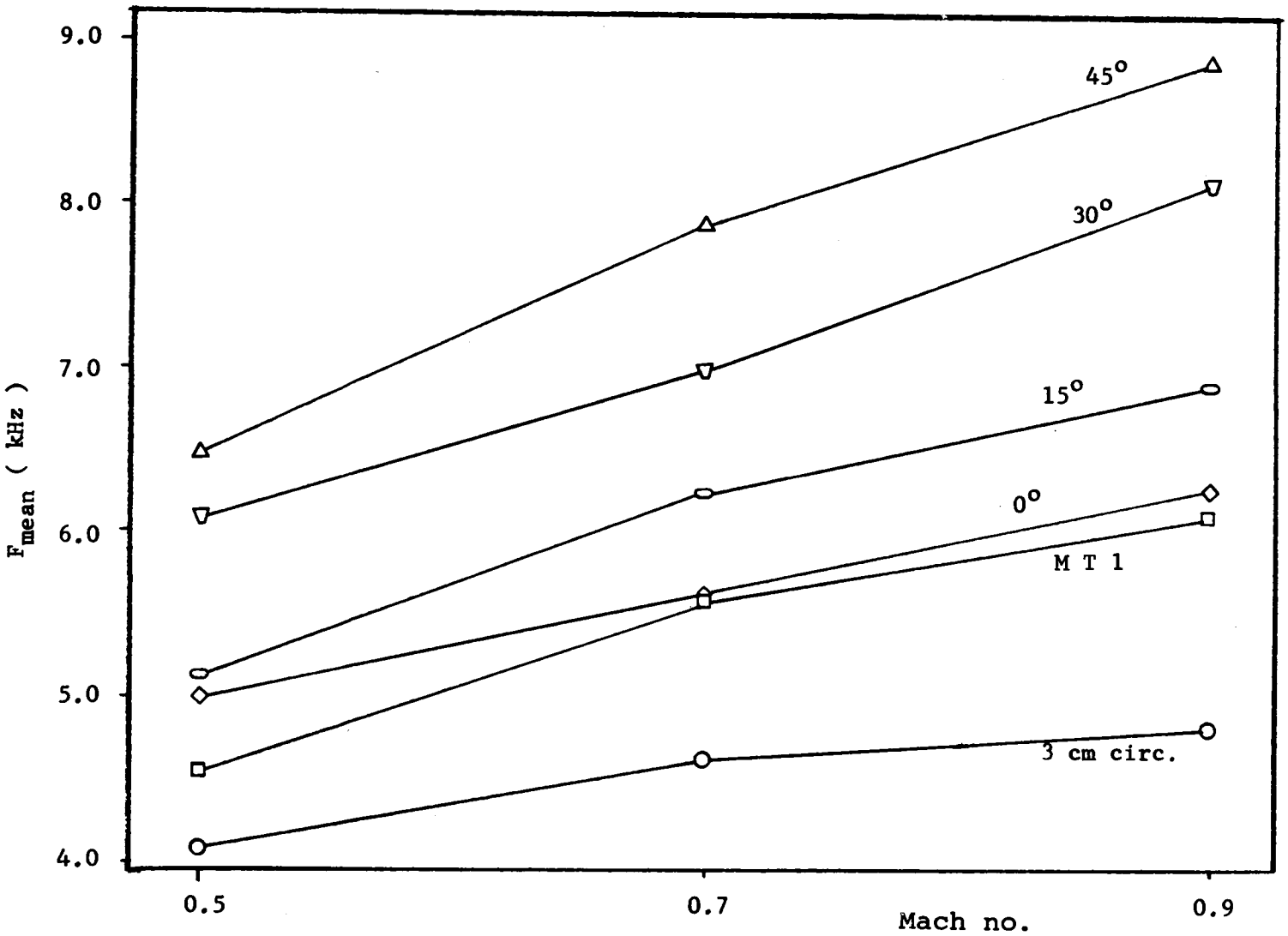


Figure 24. Noise spectra mean frequency versus Mach number for swirling flows with same sign spins and MT1 and three centimeter circular nozzles for comparison.

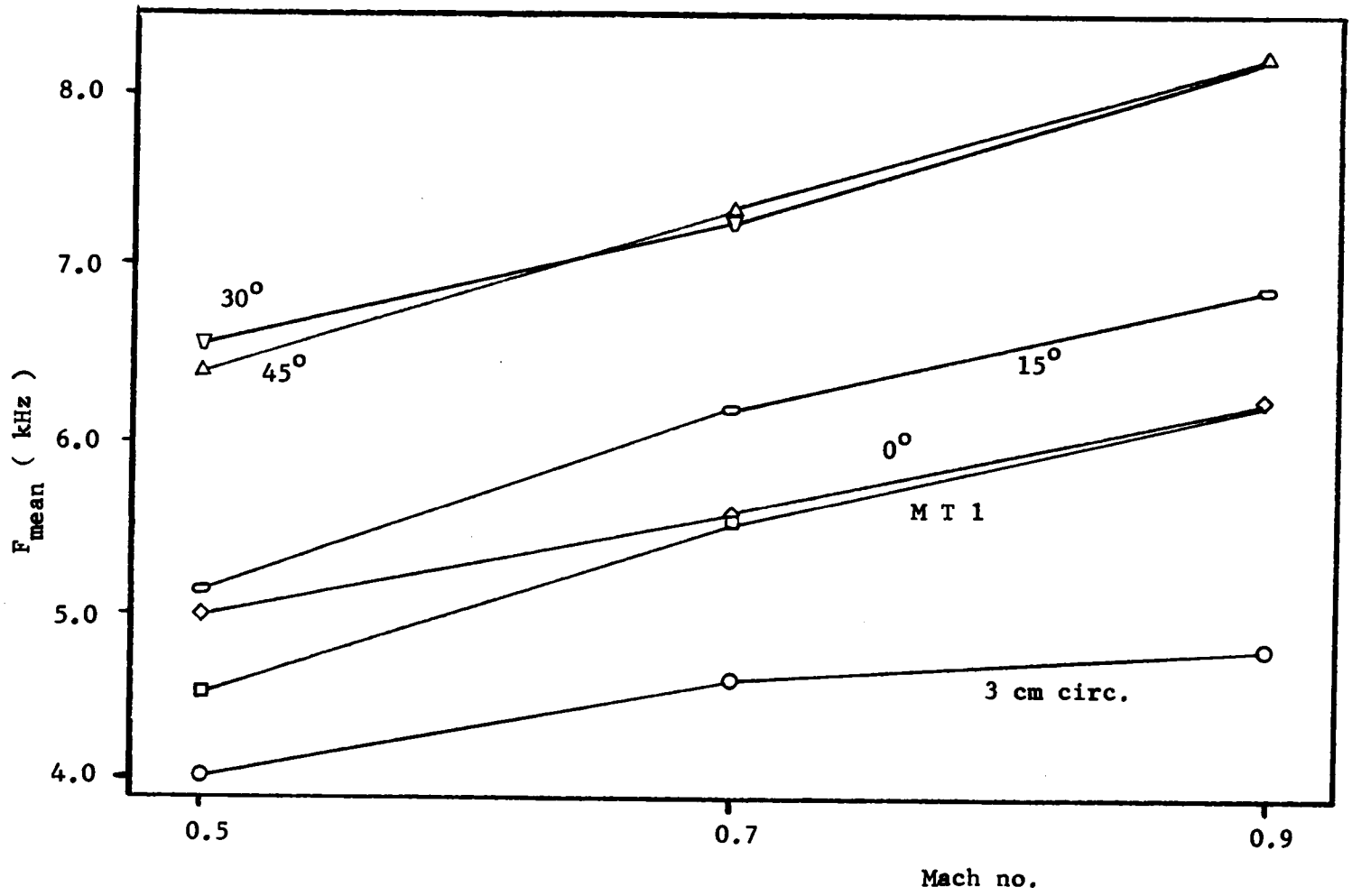


Figure 25. Noise spectra mean frequency versus Mach number for swirling flows with different sign spins and MT1 and three centimeter circular nozzles for comparison.

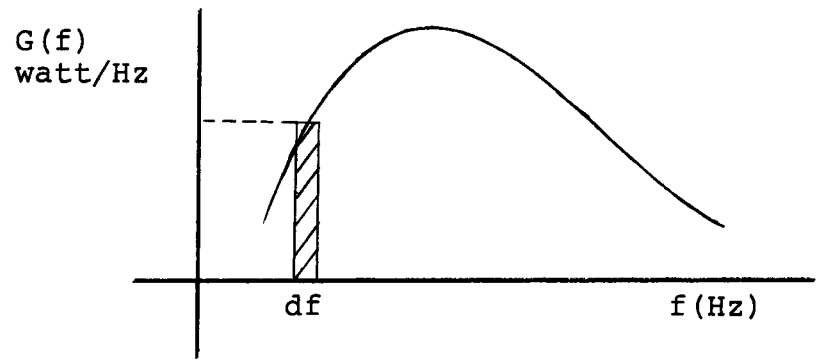


G(f) is the power spectral density function (which is the acoustic power level per Hz).

The frequency shift between the 3 cm circular nozzle and the +45+45 configuration is quite large (over 4000 Hz, from 4800 Hz to almost 9000 Hz).

The following two figures (Figures 26 and 27) are similar in information to the two previous ones except that $f_{peak}$ instead of $f_{mean}$ is now used. The definition of $f_{peak}$ is as follows: It is the frequency at which the peak SPL (dB) occurred in a frequency spectrum plot (SPL versus frequency plot). These plots show the same trend as the two previous ones for the configurations with same type spin. Again the same sign spins are the configurations in which a higher frequency shift occurs. The +45+45 configuration goes up to $f_{peak}$ = 7000 Hz ($M_e$ = 0.90) as can be seen on Figure 26, whereas the +45-45 peaks at only 5000 Hz (Figure 28). These plots are part of the actual data collected in the reverberation room.

Based on the calculations and assumptions of

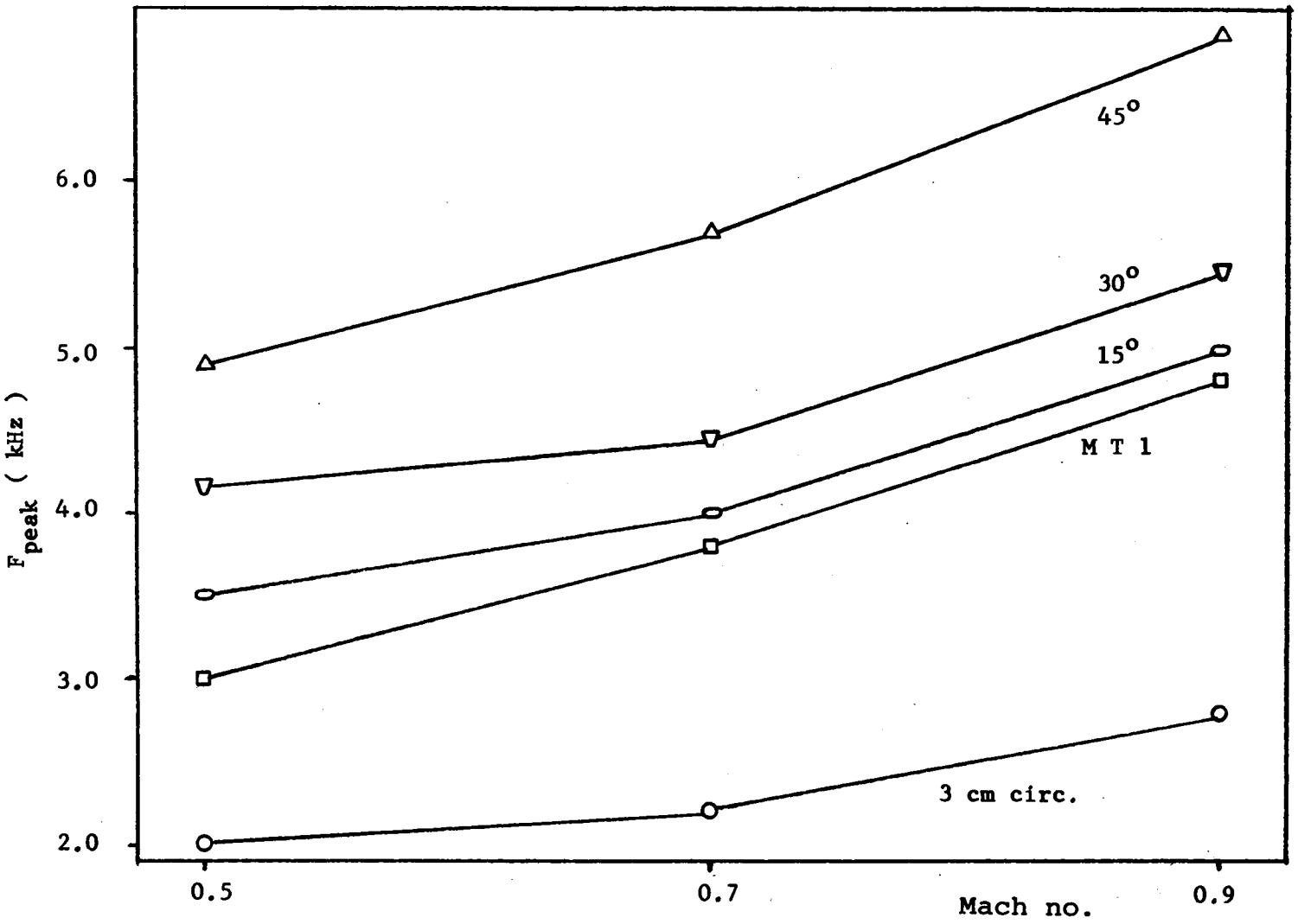


Figure 26. Noise spectra peak frequency versus Mach number for swirling flows with same sign spins and MT1 and three centimeter circular nozzles for comparison.

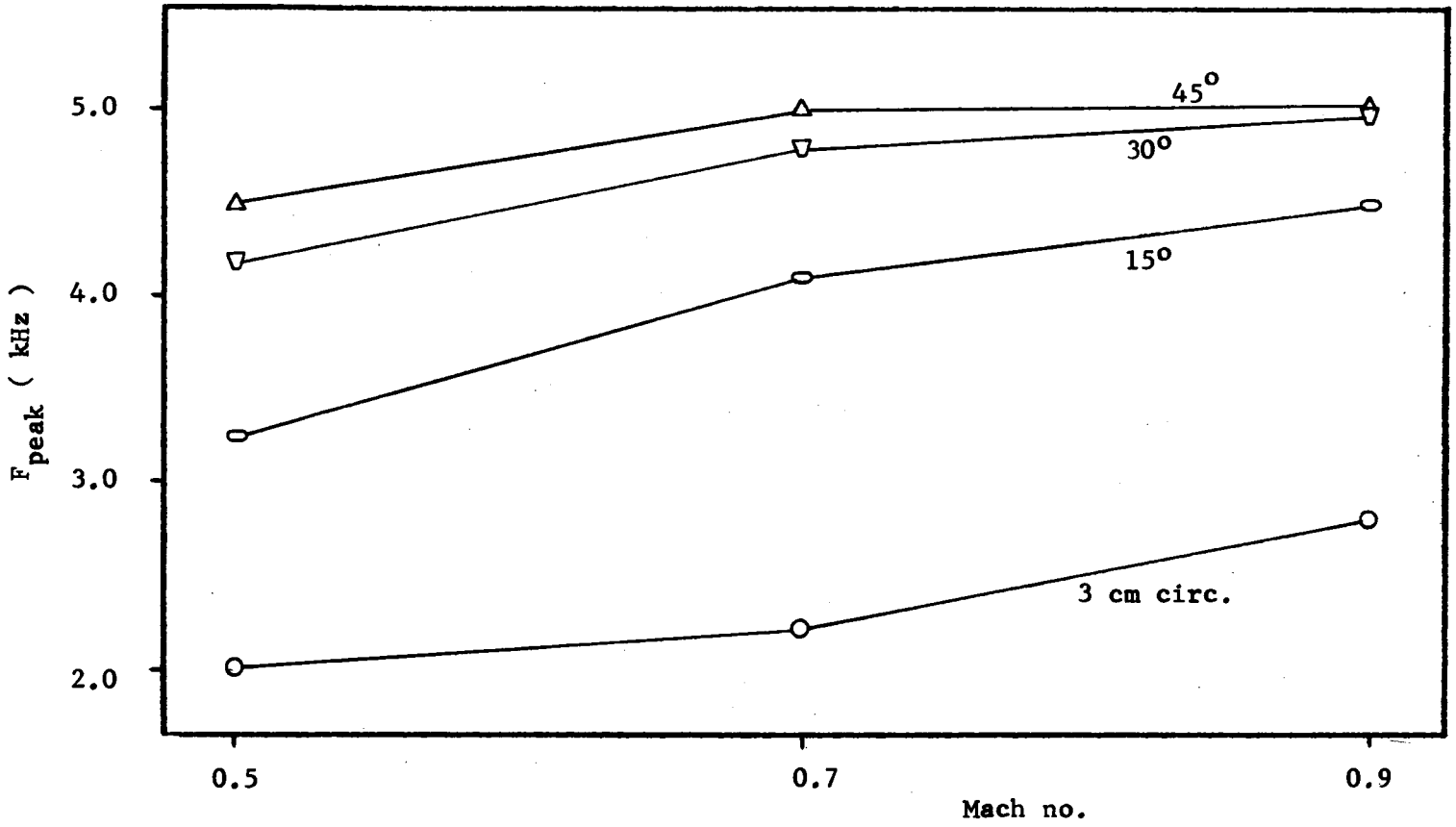


Figure 27. Noise spectra peak frequency versus Mach number for swirling flows with different sign spins and the three centimeter circular nozzles for comparison.

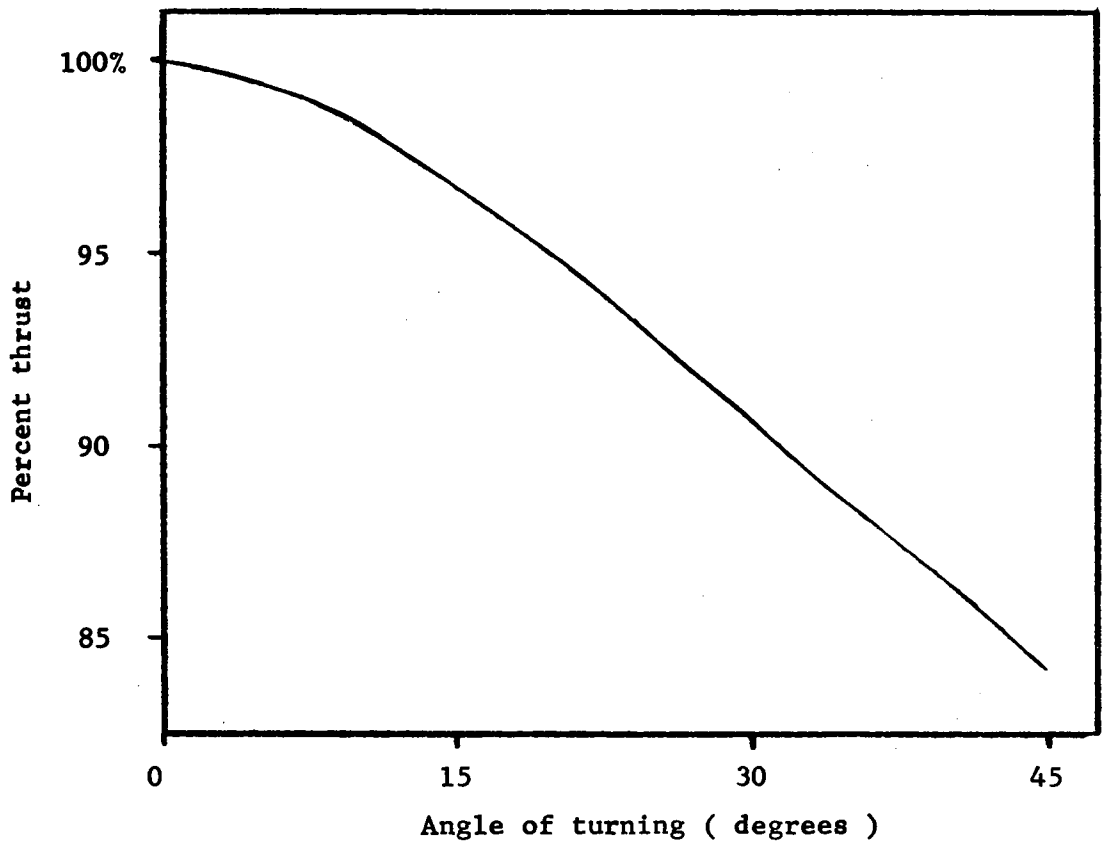


Figure 28. Thrust decrease with swirling flow.

Chapter II it was possible to estimate the thrust loss, in the flow, due to swirl. The percent thrust versus angle of swirl (up to 45 degrees) is shown on Figure 28. Low values of swirl (up to 7.5 degrees only) reduce thrust by as much as 1 percent but a value of 45 degrees of swirl would imply a thrust loss of the order of 16 percent which is quite large.

Another significant plot is shown on Figure 29 where the mass flow rate (obtained from orifice plate calculations) through the nozzles is plotted versus pressure ratio. Pressure ratio ($P_{ratio}$) was used instead of Mach number because, strictly speaking, Mach number is only applicable to the circular nozzle and the MTI since $M_e$ is calculated assuming isentropic expansion from stagnation conditions. Due to the presence of the plate the actual $M_e$ at the exit of the swirling nozzles should be somewhat lower.

Again only the 45 degree configurations were plotted because the differences in mass flow rates are quite small for swirling flows; the 15 and 30 degree data would fit somewhere in between the 0 and the 45 degree configurations (with the 30 degree closer to the 45 degree plot). For clarity in the figure they were not included.

Also differences in types of swirl (++ and +-) do not affect the mass flow which depends only on the angle of swirl. For the values of the mass flows refer to Appendix E. The following hold approximately true:

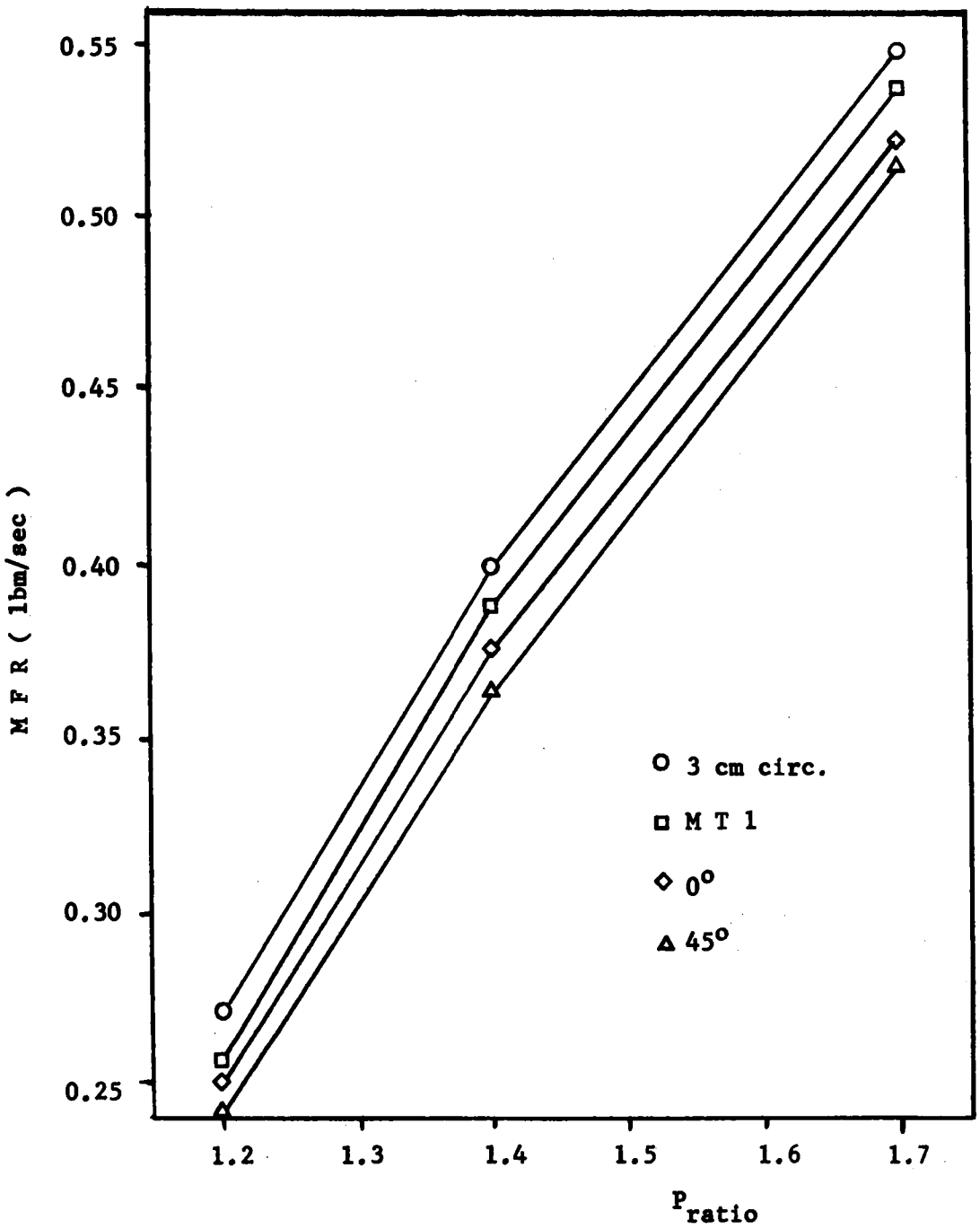


Figure 29. Mass flow rate versus pressure ratio for several nozzle configurations.

$P_{ratio} = 1.2 \Rightarrow M_e \simeq 0.5$

$P_{ratio} = 1.4 \Rightarrow M_e \simeq 0.7$

$P_{ratio} = 1.7 \Rightarrow M_e \simeq 0.9$

The shadowgraph flow photographs help to better understand the turbulent mixing of the jets. The film plates used for the shadowgraphs were placed at a distance of about 4" from the jet exit, so that only the turbulent structure was visible. Figure 30 shows only the upper half of a +45+45 and, for comparison, the upper part of an MT1. The mixing regions could not be seen too clearly but excellent shots of the spreading of the jets were obtained.

Again only the 45 degree configuration was used as being the most representative of the swirl jets. Also those two shots were chosen because they were the most clear and with the best contours.

To assure accurate data some of the tests were duplicated to check repeatability. Also one nozzle was selected as being a standard for comparing different runs. This nozzle was the multitube two (MT2) on which extensive data were already available. This nozzle was not, however, used in the acoustic discussions but it was used as a reference throughout the test runs. Differences found in PWL (dB) for any nozzle configuration, run in different days, are of the order of ±1/4 dB.



a) Without swirl, one nozzle only

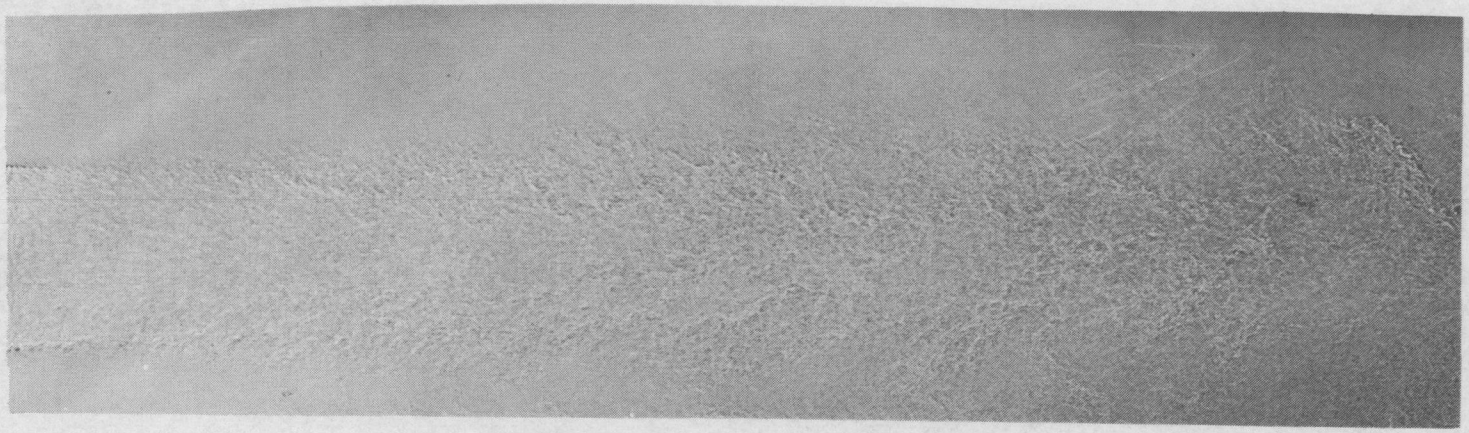

b) With swirling flow, one nozzle only (+45+45)

Figure 30. Effect of swirl in the flow field.

# III. FREE-FIELD DATA

The microphone sweeps and the frequency spectra were taken at a radius of 13 ft from the jet nozzle exits. At this radius, the lower limiting frequency at which the SPL (dB) can be measured has to have a wavelength of 13 ft or less (i.e., to satisfy far-field condition).

According to this, then

$$f = \frac{\text{speed of sound}}{\text{wavelength}} = \frac{1100}{13} = 85 \text{ Hz}$$

For all the data presented, the lowest frequency used was 250 Hz which is a safe value (three times higher) than the minimum given above. It also standardizes both free-field and reverberation room data, since the latter one also starts at a frequency of 250 Hz.

All data collected in the free-field were taken with practically no wind (wind gusts, if any, did not reach above 3 mph). The relative humidity while the tests were conducted ranged from 55 to 67 percent.

Directivity plots in two planes of symmetry (XY and XZ planes, see Figure 14, page 34) were taken. Also frequency spectra at the three different angles of sweep of +30, +60 and +90 degrees were also recorded. Only these three angles were analyzed (and not -30 degrees, for example) since all nozzle configurations under study are symmetrical, so there was no need for repetitive plots. All data were taken at a single Mach number of 0.90.

In Figures 31 and 32 the overall sound pressure (OASPL, dB) directivity is plotted for the 3 cm circular nozzle, the MT1 and the +45+45 configuration (this last one as being the most representative of the swirling flows).

As expected, the directivity patterns of the 3 cm circular nozzle and the MT1 were quite similar (particularly noticeable on Figure 32), the MT1 being the quietest of the two. The multitube is really quieter on-axis (i.e., between an angle of sweep of +30 to -30 degrees) as compared to the 3 cm circular nozzle. When comparing the directivity plots, the MT1 is practically identical to the 3 cm circular nozzle in the XZ plane (in a region of +30 to +90 and -30 to -90 degrees), but for the same region and in the XY plane the MT1 seems to be quieter by 1-2 dB. This indicates that some jet to jet shielding is taking place in the XY plane (which is the plane of the two nozzles).

The +45+45 configuration came out surprisingly high, considering the reverberation room tests, with OASPL (dB) values higher by as much as 6 dB at certain angles. But in the neighborhood of the jet axis (region of +30-30 in the directivity plots) it had a very rapid decay with a minimum at the jet centerline.

It should be noted that the three configurations tested were symmetrical in the XY and XZ planes. The directivity plots showed this to be true to within -0.5 to +2.0 dB (OASPL). A high value of +2.0 dB (OASPL) can be due to ground reflections of the sound, since the microphone,

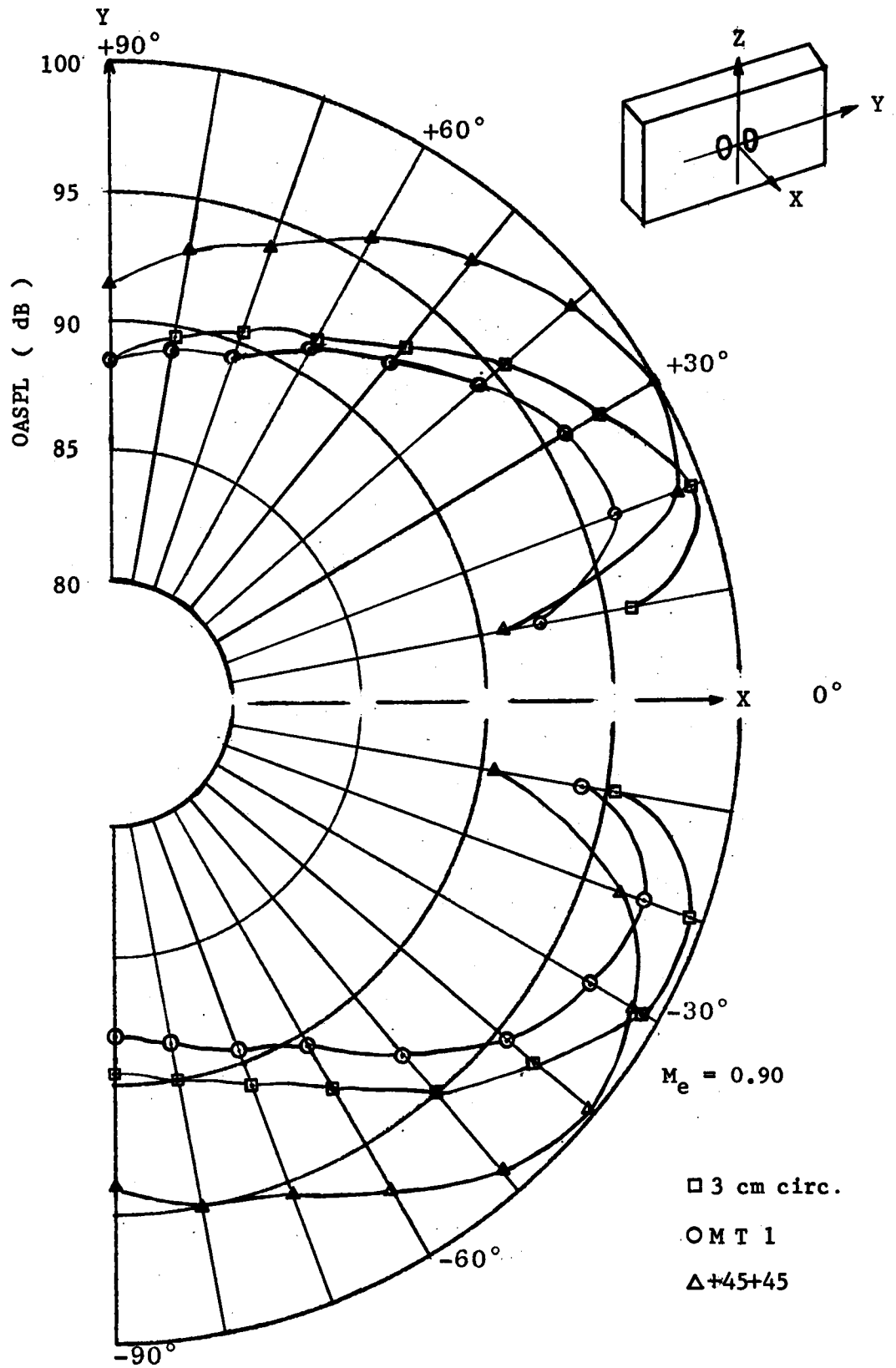


Figure 31. Sound pressure directivity in the XY plane of the multitube nozzles.

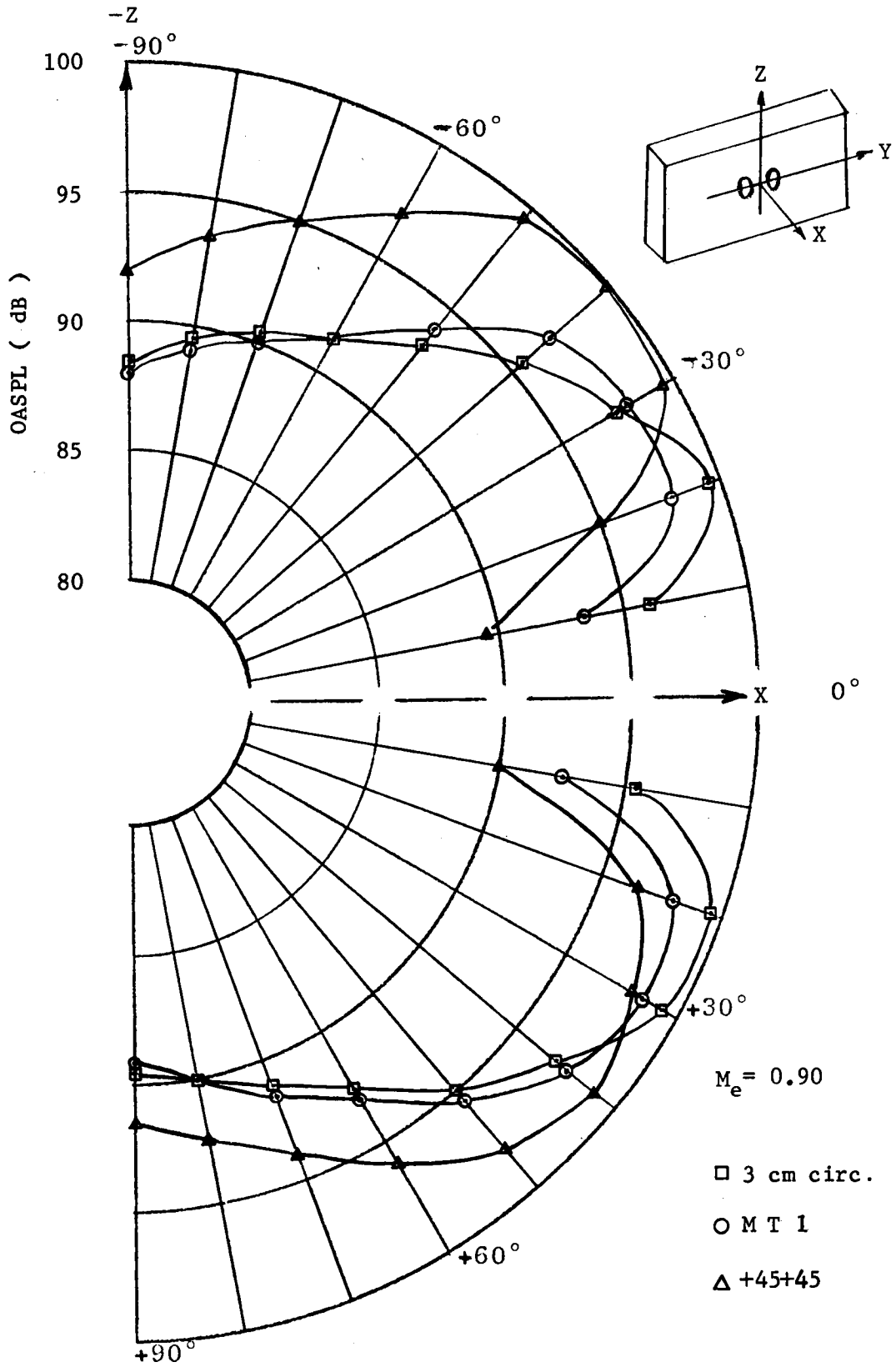


Figure 32. Sound pressure directivity in the XZ plane of the multitube nozzles.

during its sweep, approaches the ground (reflecting surface) after passing through the jet centerline region.

It is also important to realize that these free-field noise survey tests were conducted utilizing half of the sphere (with 13 ft radius and center at the jet exit) of the radiation of sound from the jets. No attempt was made to investigate the jet noise behind the nozzle exits. This could account for the higher-than-expected OASPL (dB) values of the +45+45 configuration.

The frequency spectra plots (Figures 33 to 38) agreed very well with the overall values and also the data taken in the reverberation room. In general the +45+45 configuration was the quietest at low frequencies (below 2-3 kHz) but it was considerably louder than the MT1 and the 3 cm circular nozzle above that frequency.

Also below 2-3 kHz the single circular nozzle was the loudest. The quietest nozzle at high frequencies was usually the 3 cm nozzle but the MT1 was a very close second being sometimes even lower at the high end, than the single circular nozzle (Figures 36 and 37).

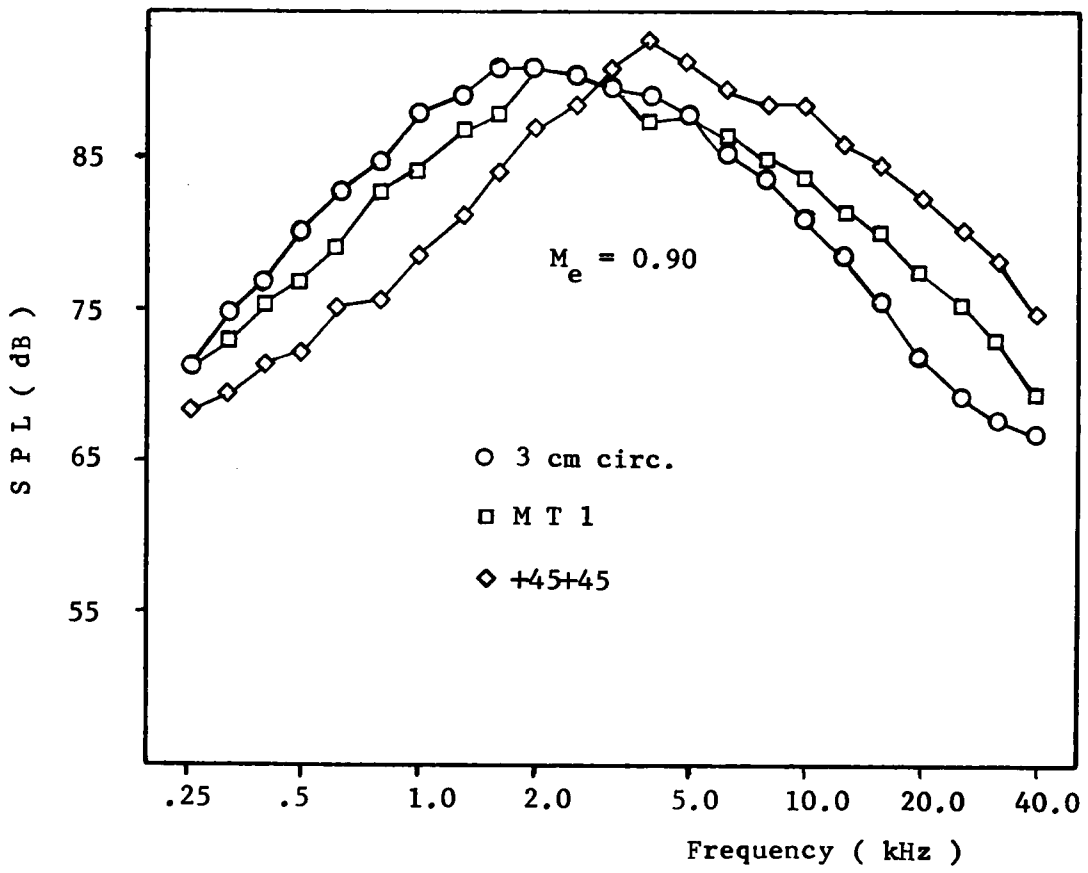


Figure 33. Frequency spectra at +30 degrees in the XZ plane.

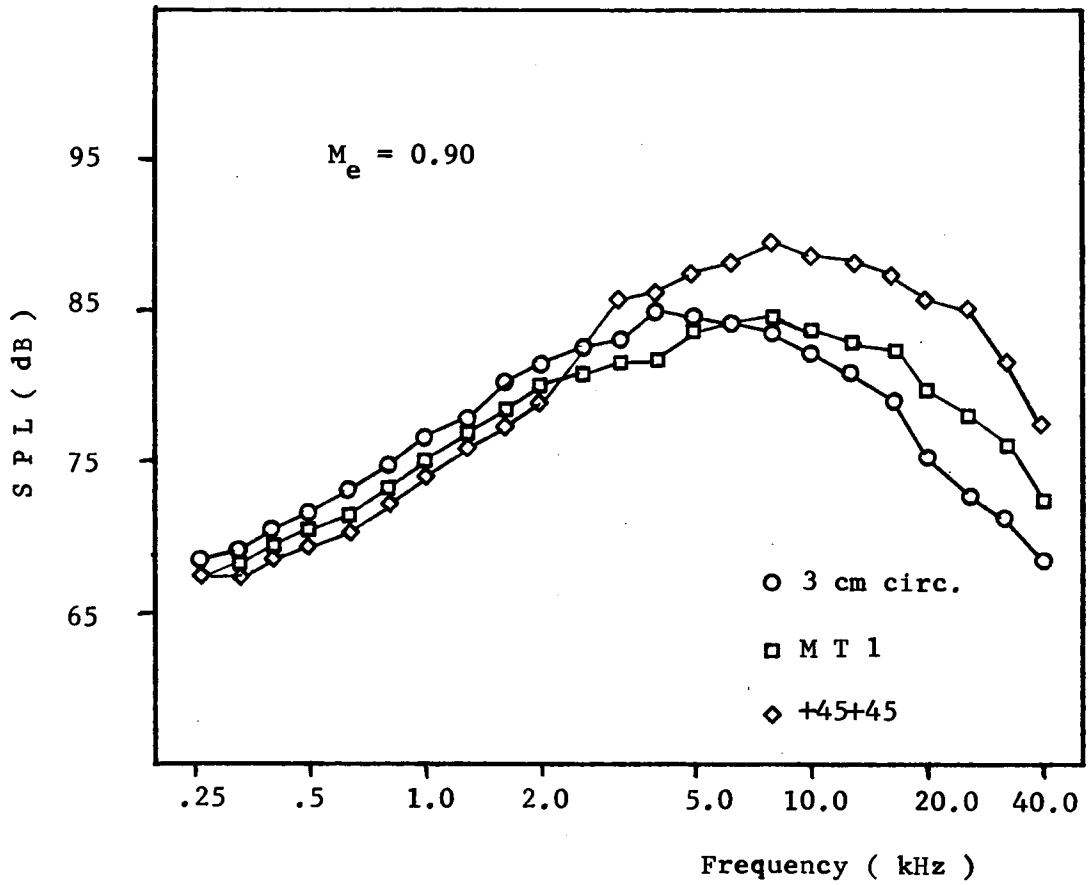


Figure 34. Frequency spectra at +60 degrees in the XZ plane.

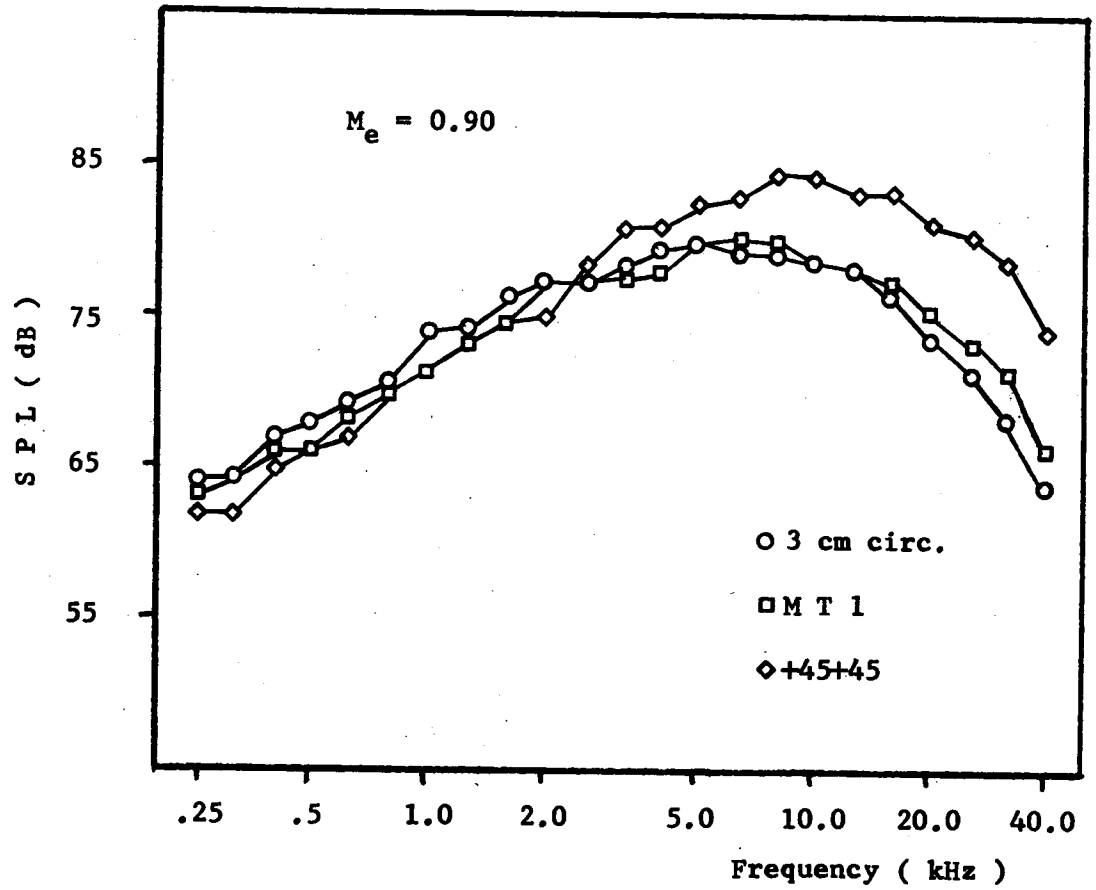


Figure 35. Frequency spectra at +90 degrees in the XZ plane.

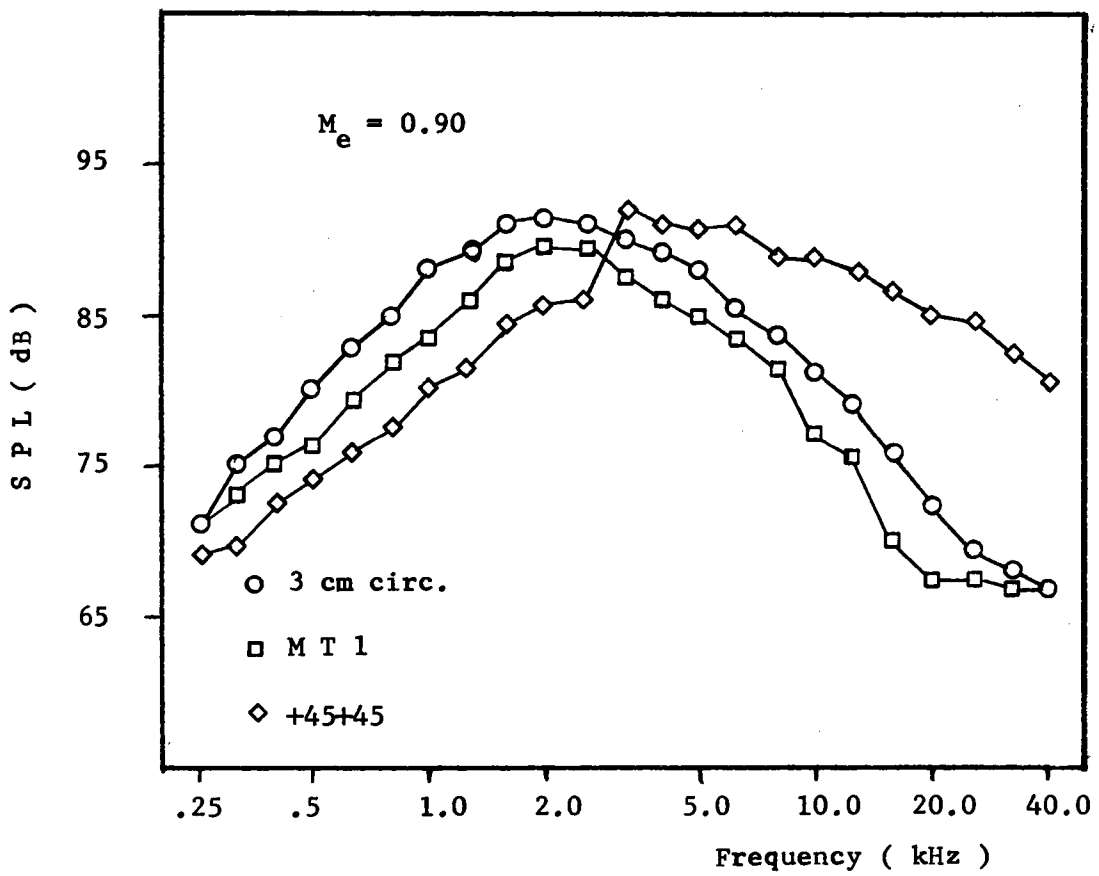


Figure 36. Frequency spectra at -30 degrees in the XY plane.

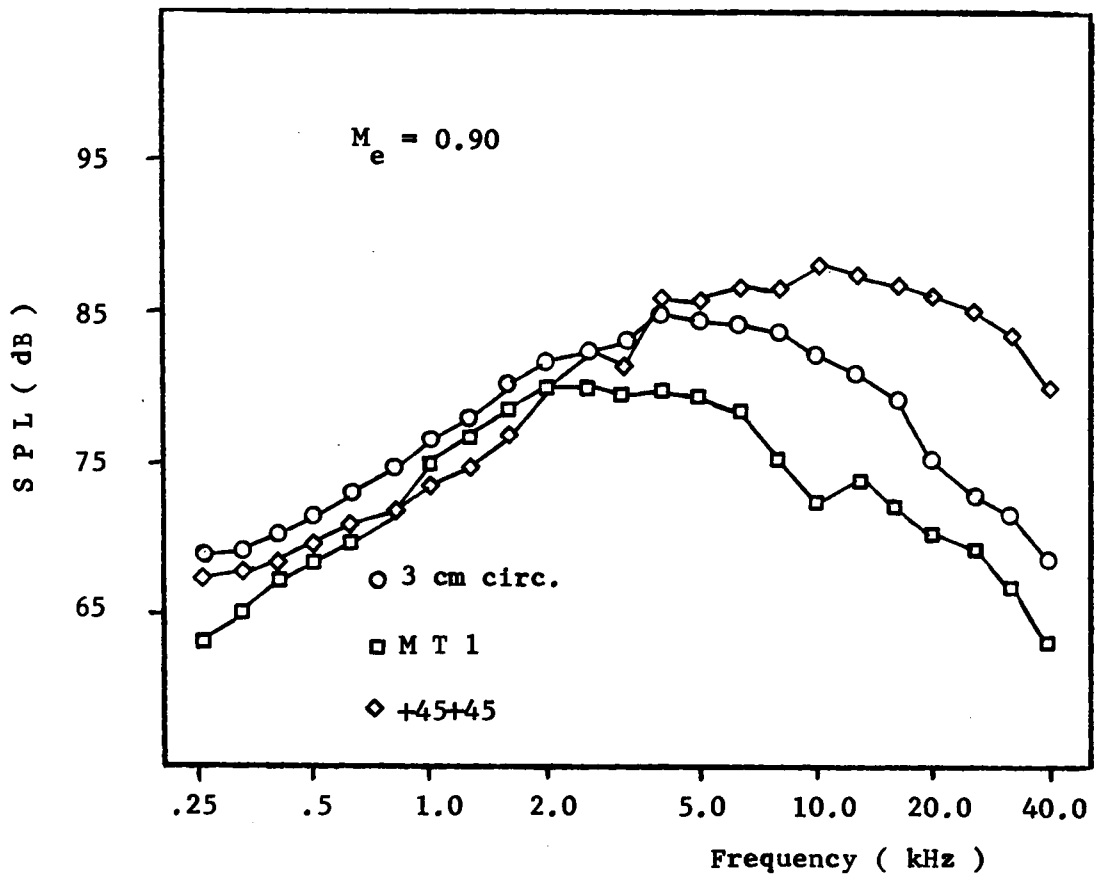


Figure 37. Frequency spectra at -60 degrees in the XY plane.

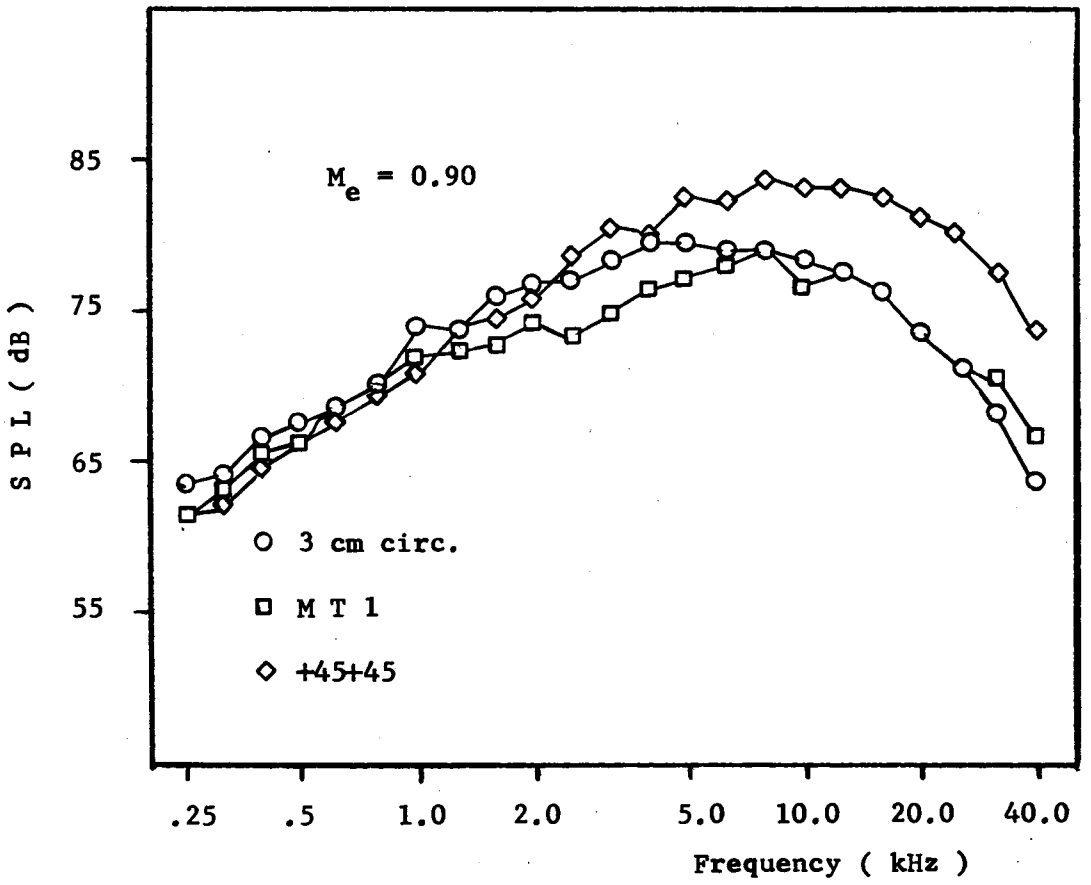


Figure 38. Frequency spectra at -90 degrees in the XY plane.

# CHAPTER V

# DISCUSSION, CONCLUSIONS AND RECOMMENDATIONS

## I. DISCUSSION OF RESULTS

### Reverberation Room

By analyzing Figures 18, 19, and 20, pages 45, 46, and 47, the following conclusions can be drawn:

1. The nozzles with different sign spins must have a peak PWL (dB) at an angle of swirl right around 30 degrees. Above this value of 30 degrees the sound power generated by this configuration decreases (at all three Mach numbers).

2. The nozzles with the same sign spins seem to have finally reached a peak PWL (dB) somewhere in the 30-45 degree swirls region and at high subsonic Mach numbers.

This is a very useful property to know since the 3 cm circular nozzle has practically the same total sound power output as the +45+45 configuration at $M_e = 0.90$. There is, however, a net gain in the rotated flow since the +45+45 generates mostly in the high frequencies range (see Figures 24 through 27, pages 52, 53, 55, and 56).

The simple multitube nozzle (MT1) was the quietest analyzed and it had no measurable thrust loss when compared with the 3 cm circular nozzle (see Appendix F).

The multitube has a small but nevertheless important frequency shift on the sound power. This is due mostly to

smaller nozzle diameters (of the twin multitubes) and to a very intense mixing of the two jets in the common mixing region (see Figure 1, page 6).

The nozzles with the same sign spins have higher shear forces in the mixing region since they look as follows:

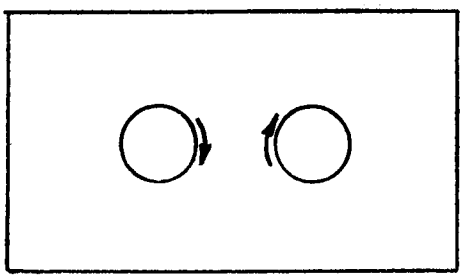

The arrows indicate the rotation of the flow. In between the two nozzles the flow will be swirling in opposite directions (high shear).

For the configurations with different sign spins there is lower shear in between the two nozzles:

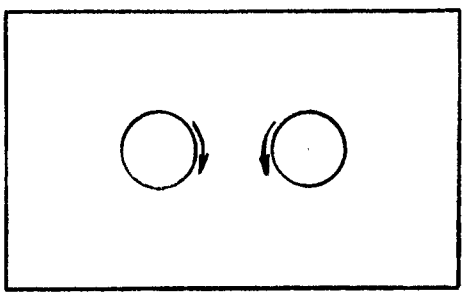

In this last case the arrows in the middle of the figure are in the same direction (low shear).

Figure 23, page 51, now shows the effect that the two different types of swirl have on the total sound power radiated: the +45+45 nozzle has, in general, a lower sound power at frequencies below 5 kHz since a more intense mixing occurs with this configuration.

It is believed that in the mixing region there is a break-up of large scale eddies into smaller ones yielding a decrease in the low frequency content and an increase of the high frequency noise. This is more so with the rotated flows since with their wider spreading angle (Figure 30, page 61) the intermixing is then increased to an even higher degree. Furthermore if the rotated flow is of the same sign spin type, then very high shear will occur at the point where the two jets intersect, causing a break-up of the large scale eddies.

But this frequency shift is obtained at the expense of net thrust, since the energy to rotate the flow comes from the kinetic energy of the jets. This thrust loss will be of about 15.8 percent for the 45 degree swirls when compared with the circular nozzle. This is a very large figure.

Also, when comparing this type of noise reduction nozzle with others (1) it can be found that, from the flight hardware viewpoint, this arrangement is highly preferable for a single nozzle with swirl since it would have a zero external in-flight drag whereas some other configurations add a considerable extra bulk and drag to the airplane (i.e., effectively decreasing the total propulsive thrust).

The mass flow rate (MFR) versus pressure ratio plot, Figure 29, page 59, shows which nozzles present the highest (45 degrees) and the lowest (3 cm circular) internal resistance to the flow. As expected, the 3 cm circular had the highest mass flow rate since it does not have any guide vanes and also its exhaust area divided by the perimeter of the nozzle exit is lower than the MT1, therefore minimizing boundary layer effects at the jet exit.

The guide vanes, themselves, decreased the nozzle exit area by about 4.1 percent. Additional boundary layer effects on the vanes could account for even further decrease in the mass flow rate.

Free-Field

From Figures 31 through 38, pages 64, 65, and 67 through 72, some important conclusions can be drawn:

1. The MT1 nozzle presents a small reduction in OASPL (dB) and an important frequency shift of the sound to the higher frequencies, when compared with the 3 cm circular nozzle.

2. The +45+45 configuration shifts the noise to very high frequencies (some peaks occurring as high as 10 kHz) with an increase of OASPL (dB).

The frequency shift, in both nozzles above, can be used to our advantage since (1) high frequencies are more easily dampened by the atmosphere; and secondly (2) they can be shielded from a ground observer in the cases where the

engines are mounted over the wings. In this last case 2, the fly-over (XZ plane) and sideline (XY plane) noise could be alleviated.

Also, from Figures 31 and 32, pages 64 and 65, it can be easily seen that the +45+45 configuration has a peak OASPL (dB) at around ±40 degrees and a sharp decline around the jet centerline. The higher spreading of the velocity peaks outward achieved with this configuration plus a high decay of velocity with distance, along the jet centerline, account for this behavior.

## II. SUMMARY

Repetitive plots (i.e., ones that show similar trends to other graphs already included) were avoided as much as possible, since they will tend to burden the reader without adding any new information. The material is, however, discussed in detail to avoid the omission of any points.

It is very important to realize that the guide vanes themselves play an important role in the noise generated downstream from the jet exit, since they effectively modify the air flow around them.

If a discontinuity (or lack of it) is present in the early history of a flow, it may change the sound output of a jet. Due to several problems encountered in the making of the guide vanes (i.e., achievement of a correct contoured shape and exact turning angle), some of the vanes offered a very smooth transition to the flow whereas some others were

not so perfectly finished. These were very small differences but they could explain why some of the data points did not quite follow the expected trends.

From a flight hardware viewpoint the multitube nozzle exit approach (without swirl) is very promising since it can be used to quiet existing engines with virtually no thrust loss (except maybe a minimal ducting loss), and has very low in-flight external drag, minimal flight weight increase and low cost.

If an aircraft possesses means of shielding high frequency noise from the ground, then a multitube nozzle with rotating (swirling) flow may be useful. This would reduce the annoyance caused by the nozzle exit flow, at the expense of thrust.

The multitube nozzles with spin (particularly with the same sign spin) seem to be very effective "frequency converters" as they shift the low frequency noise (thereby reducing it) to higher frequencies also generating some high frequency noise in this process.

## III. SUGGESTIONS FOR FUTURE WORK

Although the results of these tests were not encouraging, from a noise suppression point of view, further investigations should be conducted to better understand this problem.

It is suggested that more tests should be conducted as follows:

1. Increase the Mach number range of the tests from, at least, 0.40 to 1.0 using increments of 0.1 or smaller.

2. Use a wider range of swirl vanes (both with the same sign spins and different sign spins). Great care should be taken in the making of the swirl vanes and they should be aerodynamic shaped, if possible.

3. Utilize more multitube nozzles with different nozzle spacings.

4. Make detailed shadowgraphic study of all configurations and ranges suggested above.

5. Evaluate the static thrust of each individual nozzle configuration.

This investigation showed that this particular way of inducing swirl to the jets does not reduce (appreciably) the total sound power of a jet (at least for the angles of swirl and Mach numbers used). If any further research is to be conducted, the true values and applications of swirling flows should be assessed.

# BIBLIOGRAPHY

# BIBLIOGRAPHY


1. Coles, W. D., and E. E. Callaghan. "Full-Scale Investigation of Several Jet Engine Noise-Reduction Nozzles," National Advisory Committee for Aeronautics TN-3974, Washington, D.C., April, 1957.

2. Schwartz, I. R. "Jet Noise Suppression by Swirling the Jet Flow." American Institute of Aeronautics and Astronautics Paper No. 73-1003, October, 1973.

3. Schwartz, I. R. "Effects of Rotating Flows on Combustion and Jet Noise." American Institute of Aeronautics and Astronautics Paper No. 72-645, June, 1972.

4. Kinsler, L. E., and A. R. Frey. Fundamentals of Acoustics. New York: John Wiley and Sons, Inc., 1962.

5. Goethert, B. H., and I. U. Borchers. "Noise and Thrust Characteristics of Shrouded Multi-Nozzles of Circular Cross-Section." American Institute of Aeronautics and Astronautics Paper No. 74-45, February, 1974.

6. Yee, P. M. "An Experimental and Theoretical Investigation Concerning the Aeroacoustic Characteristics of the Rough Jet Flap." Unpublished Master's thesis, The University of Tennessee, Knoxville, 1974.

7. Harper, W. L. "An Experimental Study of the Noise Produced by Jet-Flap Type Exhausts." Unpublished Master's thesis, The University of Tennessee, Knoxville, 1971.

8. Morse, P. M., and K. U. Ingard. Theoretical Acoustics. New York: McGraw-Hill Book Company, 1968.

9. Smith, B. J. Acoustics. London: Longman Group Limited, 1971.

10. Lighthill, M. J. "On Sound Generated Aerodynamically: I. General Theory," Proceedings of the Royal Society of London, 211A:564-587, 1952.

11. Howes, W. L., and H. R. Mull. "Near Noise Field of a Jet-Engine Exhaust," National Advisory Committee for Aeronautics TN-3763, Washington, D.C., October, 1956.

12. Liepmann, H. W., and A. Roshko. Elements of Gasdynamics. New York: John Wiley and Sons, Inc., 1967.

13. Audi, M. S. "Noise Abatement by the Interaction of Cold Coaxial Model Jets." Ph.D. dissertation, Syracuse University, Syracuse, New York, 1974.

14. Gruschka, H. D. "Methods of Noise Suppression," Unpublished short course notes in Advanced Air-Breathing Propulsion Systems and Technology, The University of Tennessee Space Institute, Tullahoma, December, 1969.

# APPENDICES

# APPENDIX A

## ACOUSTIC UNITS

Since sound pressure levels range from $2 \times 10^{-5}$ N/m$^2$ for the threshold of hearing to 200 N/m$^2$ for the threshold for permanent ear damage, a logarithmic scale must be used. To have an idea of the order of magnitude of these pressure levels it is important to compare them with the average atmospheric pressure which is about $10^5$ N/m$^2$.

One defines, arbitrarily, the sound pressure level in decibels (dB), of a sound with a RMS pressure P, as

$$\text{SPL (dB)} = 10 \log (P/P_{ref})^2$$
$$= 20 \log (P/P_{ref})$$

where

$$P_{ref} = 2 \times 10^{-5} \text{ N/m}^2$$

This is therefore not an absolute scale but a relative one since a reference pressure ($P_{ref}$) must be specified.

Another unit commonly presented in dB is the sound power level (PWL). The sound power is usually measured in watts. The sound power level (dB) is then defined as

$$\text{PWL (dB)} = 10 \log (W/W_{ref})$$

where $W_{ref} = 10^{-12}$ watts and W is the RMS sound power in watts.

It is important to realize that a ΔPWL of 3 dB corresponds to half of the sound power (in watts).

## APPENDIX B

## DESCRIPTION OF INSTRUMENTATION

The following Bruel and Kjaer equipment was used in the two recording channels:

Audio Frequency Spectrometers
Channel I--Type 2112 (12.5-40 kHz)
Channel II--Type 2111 (10.0-31.5 kHz)

Level Recorders--Type 2305
Channel I--Serial No. 241148
Channel II--Serial No. 199561

Five Quarter-Inch Condenser Microphones
With Microphone Cartridge Type 4135-36, and a frequency range of 20-200 kHz, dynamic range up to 180 dB

and to calibrate the microphones:

General Radio Sound Level Calibrator, Type 1562-A
It produces 114 dB, SPL, at any of the following frequencies: 125, 250, 500, 100, 2000 Hz

The following equipment was used for the reverberation times measurement (as outlined on Figure 2, page 15):

General Radio Random Noise Generator
Type 1390-A, Serial No. 1192

Dynaco Power Amplifier
Dynakit Mark IV, Serial No. 8832857

Allied Loudspeaker
Model 615 HC, 15" Coaxial
50 Watt, 3-Way Speaker

A very simple installation (schematically shown on Figure 17, page 39) was used to take shadowgraphs. It consisted of the following:

A spark light source of very high intensity and short duration (or the order of a few microseconds),

produced by the discharge of two capacitors. It is manufactured by J. Unertl Optical Corporation.

A high voltage power supply which charged the capacitors. It is the following unit: Universal Voltronics Corporation High Voltage Power Supply.

The films and papers used in printing and developing are standard, readily available, Kodak products:

Kodak Royal Pan 4141 Film

Kodak Kodabromide F-5 Paper

The development of these films and papers was done following the manufacturer's instructions but keeping in mind that the most desirable property to achieve was to obtain the highest possible contrast.

# APPENDIX C

## TYPICAL REVERBERATION ROOM AND FREE-FIELD DATA

The following tables (Tables III and IV) are typical of the test data collected in this investigation.

TABLE III

TYPICAL REVERBERATION ROOM DATA (TEST RUN 162)

| Run | App. Mach No. | Nozzle | $T_{RR}$ (°F) | $P_{sc}$ (psf) | $P_{ups}$ (psi) | $T_o$ (°F) | $\Delta P_{orifice}$ (in. hg.) |
|---|---|---|---|---|---|---|---|
| 1 | 0.5 | 0° | 85 | 508 | 4.18 | 87 | 4.40 |
| 2 | 0.7 | 0° | 84 | 932 | 8.40 | 82 | 8.00 |
| 3 | 0.9 | 0° | 83 | 1577 | 14.30 | 78 | 11.50 |
| 4 | 0.5 | +15-15 | 86 | 511 | 4.22 | 84 | 4.40 |
| 5 | 0.7 | +15-15 | 85 | 934 | 8.40 | 81 | 7.80 |
| 6 | 0.9 | +15-15 | 84 | 1575 | 14.25 | 78 | 11.30 |
| 7 | 0.5 | -15-15 | 95 | 505 | 4.17 | 96 | 4.40 |
| 8 | 0.7 | -15-15 | 93 | 932 | 8.39 | 86 | 7.80 |
| 9 | 0.9 | -15-15 | 90 | 1575 | 14.20 | 80 | 11.40 |
| 10 | 0.5 | +30-30 | 92 | 508 | 4.11 | 84 | 4.10 |
| 11 | 0.7 | +30-30 | 90 | 935 | 8.15 | 82 | 7.30 |
| 12 | 0.9 | +30-30 | 86 | 1580 | 13.85 | 75 | 11.40 |
| 13 | 0.5 | +30+30 | 90 | 508 | 4.05 | 83 | 4.16 |
| 14 | 0.7 | +30+30 | 89 | 930 | 8.20 | 82 | 7.30 |
| 15 | 0.9 | +30+30 | 88 | 1578 | 13.85 | 78 | 11.50 |
| 16 | 0.5 | +45-45 | 93 | 505 | 4.00 | 85 | 4.10 |
| 17 | 0.7 | +45-45 | 92 | 928 | 8.19 | 83 | 7.20 |
| 18 | 0.9 | +45-45 | 88 | 1575 | 13.79 | 75 | 11.50 |
| 19 | 0.5 | MT1 | 92 | 508 | 4.28 | 83 | 4.76 |
| 20 | 0.7 | MT1 | 90 | 928 | 8.55 | 78 | 8.70 |
| 21 | 0.9 | MT1 | 88 | 1575 | 14.60 | 76 | 12.30 |
| 22 | 0.5 | +45+45 | 99 | 508 | 4.02 | 83 | 4.04 |
| 23 | 0.7 | +45+45 | 90 | 930 | 8.12 | 79 | 7.20 |
| 24 | 0.9 | +45+45 | 90 | 1570 | 13.75 | 75 | 11.40 |
| 25 | 0.5 | MT2 | 90 | 508 | 4.25 | 79 | 4.50 |
| 26 | 0.7 | MT2 | 89 | 935 | 8.55 | 78 | 8.10 |
| 27 | 0.9 | MT2 | 88 | 1570 | 14.30 | 76 | 12.30 |

TABLE IV

TYPICAL FREE-FIELD DATA (TEST RUN 168)

| Run | App. Mach No. | Nozzle | Plane of Sweep | Position in the Sweep | $P_{sc}$ (psf) | $T_o$ (°F) |
|---|---|---|---|---|---|---|
| 8 | 0.9 | MT1 | XY | sweep | 1580 | 96 |
| 9 | 0.9 | MT1 | XY | -90 | 1580 | 93 |
| 10 | 0.9 | MT1 | XY | -60 | 1580 | 91 |
| 11 | 0.9 | MT1 | XY | -30 | 1582 | 90 |
| 12 | 0.9 | MT1 | XY | +30 | 1580 | 90 |
| 13 | 0.9 | MT1 | XY | +60 | 1584 | 90 |
| 14 | 0.9 | MT1 | XY | +90 | 1580 | 90 |
| 15 | 0.9 | +45+45 | XY | +90 | 1580 | 98 |
| 16 | 0.9 | +45+45 | XY | +60 | 1580 | 97 |
| 17 | 0.9 | +45+45 | XY | +30 | 1578 | 96 |
| 18 | 0.9 | +45+45 | XY | -30 | 1580 | 95 |
| 19 | 0.9 | +45+45 | XY | -60 | 1577 | 95 |
| 20 | 0.9 | +45+45 | XY | -90 | 1580 | 94 |
| 21 | 0.9 | +45+45 | XY | sweep | 1580 | 92 |
| 29 | 0.9 | 3 cm | XZ | +90 | 1572 | 95 |
| 30 | 0.9 | 3 cm | XZ | +60 | 1572 | 94 |
| 31 | 0.9 | 3 cm | XZ | +30 | 1573 | 93 |
| 32 | 0.9 | 3 cm | XZ | -30 | 1574 | 92 |
| 33 | 0.9 | 3 cm | XZ | -60 | 1574 | 91 |
| 34 | 0.9 | 3 cm | XZ | -90 | 1572 | 90 |
| 35 | 0.9 | 3 cm | XZ | sweep | 1579 | 89 |

# APPENDIX D

## PARTIAL OUTPUT OF A DATA REDUCTION COMPUTER PROGRAM

The following results (see Table V) were obtained by reducing the reverberation room data, using a computer program.

TABLE V

PARTIAL OUTPUT OF A DATA REDUCTION COMPUTER PROGRAM (SAMPLE DATA AT $M_e$ = 0.9 ONLY)

| Nozzle | PWL (dB) | MFR (lbm/sec) | Mean Frequency (Hz) | $U_e$ (ft/sec) |
|---|---|---|---|---|
| 0° | 114.4 | 0.521 | 6260 | 952.9 |
| +15-15 | 115.0 | 0.518 | 6895 | 952.4 |
| +30-30 | 116.5 | 0.514 | 8220 | 951.0 |
| +45-45 | 116.3 | 0.514 | 8220 | 949.8 |
| -15-15 | 114.6 | 0.517 | 6900 | 954.2 |
| +30+30 | 116.0 | 0.513 | 8160 | 953.1 |
| +45+45 | 115.9 | 0.512 | 8970 | 948.6 |
| MT1 | 114.2 | 0.536 | 6110 | 950.7 |
| MT2 | 113.9 | 0.531 | 6335 | 949.5 |
| 3 cm | 116.1 | 0.548 | 4810 | 944.3 |

# APPENDIX E

## ESTIMATE OF THE FREQUENCY SHIFT WITH INTERFERING AIR JETS

Assuming that the air jets expand into the ambient air with a half-angle of 9.4 degrees (1), it is possible to estimate which frequencies will be mostly affected by this interference mixing (refer to Figure 1, page 6).

The high frequency part of the noise spectrum is generated near the nozzle exit. Lower frequencies are generated further downstream (14).

By simple geometrical considerations the distance downstream where the two jets impinge can be found. Using this value in Figure 39, from Reference (11), it is possible to determine the predominant sound frequency at the point where the jets impinge, since the curve on Figure 39 was arrived at by comparing the locations of the maximum levels associated with a given frequency therefore locating the acoustic sources according to the frequency (11).

It can be found that:

1. Distance at which the two jets impinge = 1.5 nozzle diameters (D = 0.835").

2. Corresponding Strouhal number $S_t$ = 0.45 (Figure 39).

But the Strouhal number equals:

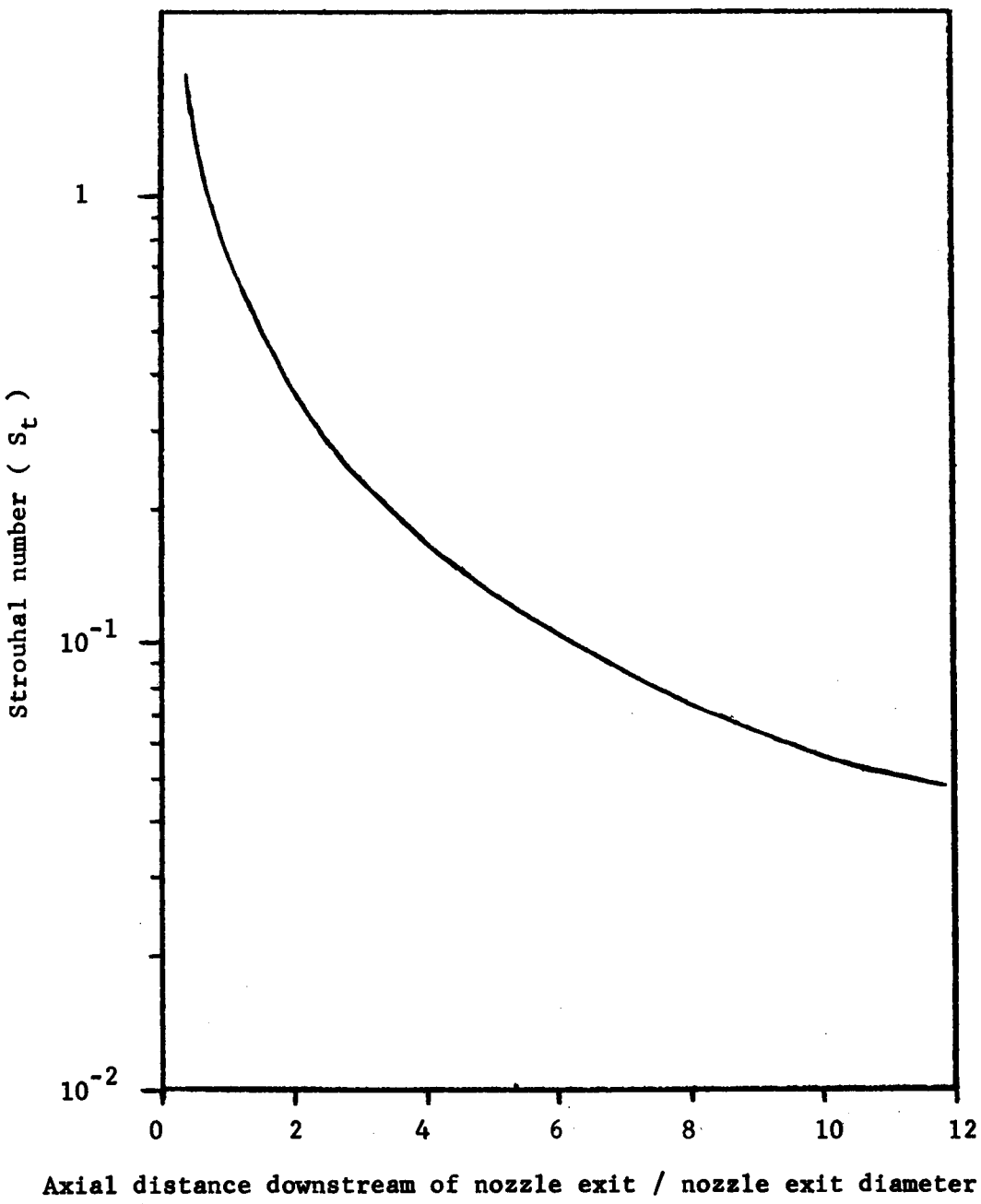


Figure 39. Strouhal number versus distance downstream.

$$S_t = f \frac{d}{U} \text{ or } f = S_t \frac{U}{d}$$

Using U = 950 ft/sec and d = 0.835/12 ft then:

$f \simeq 6000$ Hz

# APPENDIX F

## ACTUAL THRUST MEASUREMENTS ON THE MT1 AND THE THREE CENTIMETER CIRCULAR NOZZLE

In order to investigate the order of magnitude of thrust loss (or gain) some static thrust measurements were conducted to compare (only) the 3 cm circular nozzle and the MT1.

The test set-up was very simple as the air jets were made to impinge perpendicular to a flat plate. The force exerted on the plate, by the jets, was then a measure of the thrust of those jets.

This is a somewhat crude approach to thrust measurement and was primarily to give only an order of magnitude of the thrust of both jets.

In those measurements, the thrust of both jets was found to be the same to within ±2 percent, for a Mach number range of $0.5 \leq M_e \leq 0.9$.

## APPENDIX G

## SOLUTION OF EQUATION 20, CHAPTER II

Equation 20 was solved, using a computer program, for the following case (flow at $M_e = 0.9$):

$2r = 0.835"$

$\Delta z = 0.75"$

$V_o = 943.69$ ft/sec

$T_o = 453.2$ °R

$R = 53.34$ ft-lbf/lbm °R

$C_p = 0.24$ BTU/lbm °R

To make Equation 20 dimensionally correct, R (gas constant) and $C_p$ (specific heat at constant pressure) had to be multiplied by the following:

$$R = 53.34 \text{ ft-lbf/lbm °R} \cdot 32.174 \text{ lbm-ft/lbf-sec}^2$$
$$= 53.34 \cdot 32.174 \text{ ft}^2/\text{°R-sec}^2$$

$$C_p = 0.24 \text{ BTU/lbm °R} \cdot 777.5 \text{ ft-lbf/BTU} \cdot 32.174 \text{ lbm-ft/lbf-sec}^2$$
$$= 0.24 \cdot 777.5 \cdot 32.174 \text{ ft}^2/\text{°R-sec}^2$$

In Figure 28, page 57, the results for this particular case are plotted.

# VITA

João Paulo Trincheiras Tôrres was born in Lisboa, Portugal on March 10, 1952. He attended elementary schools in that city and graduated from Liceu Nacional de Oeiras in July, 1969. The following October he entered Instituto Superior Técnico Lisboa, Portugal. In September, 1970, he transferred to The University of Bridgeport, Bridgeport, Connecticut, and in December, 1972, he received a Bachelor of Science degree in Mechanical Engineering.

He entered the Graduate School at The University of Tennessee Space Institute in January, 1973, where he held a Research Assistantship. He received a Master of Science degree with a major in Aerospace Engineering in December, 1974.

He is a member of the American Institute of Aeronautics and Astronautics.